Journal of Pharmaceutical Analysis 14 (2024) 177–195

Contents lists available at ScienceDirect

Journal of Pharmaceutical Analysis

journal homepage: www.elsevier.com/locate/jpa

Original article

Gut microbiome-based thiamine metabolism contributes to the protective effect of one acidic polysaccharide from *Selaginella uncinata* (Desv.) Spring against inflammatory bowel disease

Haochen Hui [a], Zhuoya Wang [a], Xuerong Zhao [a], Lina Xu [a], Lianhong Yin [a], Feifei Wang [b, ***], Liping Qu [b, **], Jinyong Peng [a, c, *]

[a] Department of Pharmaceutical Analysis, College of Pharmacy, Dalian Medical University, Dalian, Liaoning, 116044, China
[b] Innovation Materials Research and Development Center, Botanee Research Institute, Yunnan Botanee Bio-technology Group Co., Ltd., Kunming, 650106, China
[c] Department of Traditional Chinese Medicine Pharmacology, School of Pharmacy, Anhui University of Chinese Medicine, Hefei, 230012, China

ARTICLE INFO

Article history:
Received 16 April 2023
Received in revised form
28 July 2023
Accepted 7 August 2023
Available online 10 August 2023

Keywords:
Gut microbiota
Inflammatory bowel disease
Polysaccharide
Selaginella uncinata (Desv.) Spring
Thiamine metabolism

ABSTRACT

Inflammatory bowel disease (IBD) is a serious disorder, and exploration of active compounds to treat it is necessary. An acidic polysaccharide named SUSP-4 was purified from *Selaginella uncinata* (Desv.) Spring, which contained galacturonic acid, galactose, xylose, arabinose, and rhamnose with the main chain structure of →4)-α-D-GalAp-(1→ and →6)-β-D-Galp-(1→ and the branched structure of →5)-α-L-Araf-(1→ . Animal experiments showed that compared with Model group, SUSP-4 significantly improved body weight status, disease activity index (DAI), colonic shortening, and histopathological damage, and elevated occludin and zonula occludens protein 1 (ZO-1) expression in mice induced by dextran sulfate sodium salt (DSS). 16S ribosomal RNA (rRNA) sequencing indicated that SUSP-4 markedly downregulated the level of *Akkermansia* and *Alistipes*. Metabolomics results confirmed that SUSP-4 obviously elevated thiamine levels compared with Model mice by adjusting thiamine metabolism, which was further confirmed by a targeted metabolism study. Fecal transplantation experiments showed that SUSP-4 exerted an anti-IBD effect by altering the intestinal flora in mice. A mechanistic study showed that SUSP-4 markedly inhibited macrophage activation by decreasing the levels of phospho-nuclear factor kappa-B (p-NF-κB) and cyclooxygenase-2 (COX-2) and elevating NF-E2-related factor 2 (Nrf2) levels compared with Model group. In conclusion, SUSP-4 affected thiamine metabolism by regulating *Akkermania* and inhibited macrophage activation to adjust NF-κB/Nrf2/COX-2-mediated inflammation and oxidative stress against IBD. This is the first time that plant polysaccharides have been shown to affect thiamine metabolism against IBD, showing great potential for in-depth research and development applications.

1. Introduction

Inflammatory bowel disease (IBD), a common gastrointestinal disorder, includes Crohn's disease and ulcerative colitis. Statistics have shown that the incidence of IBD is rising sharply, adding to the burden of the health care system [1]. In general, IBD is thought to be the result of a combination of genetics, immunity, infection, and environment [2]. The researchers found changes in the function and composition of the gut microbiota in IBD patients, which may be key to understanding the mechanism of action of IBD [3]. Current methods for IBD treatment contain immunosuppressive agents, biological agents, and antibiotics, which can lead to serious side effects [4,5]. Therefore, it is important to find active precursors with efficient and low toxicity to treat IBD.

Gut microbiota have the roles of digesting food components, synthesizing essential vitamins, stimulating and modulating the immune system, removing toxins and carcinogens, and improving

Peer review under responsibility of Xi'an Jiaotong University.
* Corresponding author. Department of Pharmaceutical Analysis, College of Pharmacy, Dalian Medical University, Dalian, Liaoning, 116044, China.
** Corresponding author.
*** Corresponding author.
E-mail addresses: wangfeifei@winona.cn (F. Wang), quliping@winona.cn (L. Qu), jinyongpeng2005@163.com (J. Peng).

https://doi.org/10.1016/j.jpha.2023.08.003

intestinal function [6,7]. The key modes of interaction between the intestinal flora and host are through flora metabolism, and flora metabolites are essential for life activities [8]. The joint study of intestinal flora and metabolites is extremely valuable for the action of drugs.

Plant polysaccharides have received considerable attention. Numerous investigations have verified that polysaccharides have antitumor [9], antioxidant [10], anti-inflammatory [11] and hypoglycemic [12] effects. However, the weakly acidic environment in the stomach does not allow the full decomposition and utilization of polysaccharides, while the intestinal flora has an extremely strong decomposition effect [13]. Some polysaccharides from Scutellaria baicalensis [14], Ganoderma lucidum [15], Hawthorn [16], and Aloe vera [17] have been shown to treat IBD by improving intestinal flora and metabolite levels.

Selaginella uncinata (Desv.) Spring (*S. uncinata*), with the effect of relieving cough and dampness, clearing heat, and detoxifying, has been used to treat jaundice, dysentery, cholecystitis, enteritis, diarrhea, rheumatic joint pain, and burns [18]. The chemical constituents of *S. uncinata* include mainly flavonoids [19] and steroidal saponins [20]. In our previous study, we demonstrated three polysaccharides from *S. uncinata* with anti-inflammatory activities by detecting lipopolysaccharides (LPS)-induced release of inflammatory factors in THP-1 macrophages [21]. However, there have been no reports of polysaccharides from *S. uncinata* against IBD. In this study, polysaccharides from *S. uncinata* were purified and characterized, and their biological activity against IBD was explored by sequencing the gut microbiota and metabolomics.

2. Methods and materials

2.1. Materials

S. uncinata was provided by Qiancaoyuan Pharmaceutical Co., Ltd. (Yunnan, China). DEAE-52 cellulose, Sephadex G-75, and dialysis bags (3500 D) were provided by Solarbio (Beijing, China). Sodium acetate trihydrate, sodium hydroxide, and standard monosaccharides were obtained from Sigma (St. Louis, MO, USA). Methanol and trifluoroacetic acid (TFA) were provided by ANPEL Laboratory Technologies (Shanghai) Inc. (Shanghai, China). Dextran sulfate sodium was obtained from Macklin (Shanghai, China). A bicinchoninic acid assay (BCA) kit, rapid blocking solution, antibody diluent, 6× loading buffer, and marker protein (10–180 kDa) were purchased from Sevenbio (Beijing, China). Antibodies against zonula occludens protein 1 (ZO-1), occludin, nuclear factor kappa-B (NF-κB), phospho-nuclear factor kappa-B (p-NF-κB), NF-E2-related factor 2 (Nrf2), cyclooxygenase-2 (COX-2), cluster of differentiation 68 (CD68), CD86, and glyceraldehyde-3-phosphate dehydrogenase (GAPDH) were purchased from Proteintech (Wuhan, China). Vancomycin, ampicillin, metronidazole, LPS, and thiamine (THA) were purchased from MedChemExpress (Shanghai, China).

2.2. Extraction of SUSP-4

Using a 20:1 water/plant ratio at 95 °C for 2 h, the powders (20–40 mesh) of the plant were extracted with water, and the supernatant was collected and concentrated. Then, 95% ethanol was added to precipitate the extract. In a vacuum drying oven, the precipitate was dried and ground into powder, producing crude polysaccharide (SUSP).

One hundred milligrams of SUSP dissolved in water (10 mg/mL) was added to a DEAE-52 cellulose column. A NaCl solution (0, 0.1, 0.2, and 0.3 M) was used to elute the column at a rate of 1 mL/min. In each tube, 10 mL of eluent was collected, and the absorbance at 490 nm was measured. The fraction of SUSP-0.3 was combined, concentrated, dialyzed, and freeze-dried. It was eluted with purified water at 1 mL/min after 50 mg of SUSP-0.3 (10 mg/mL) was added to the Sephadex G-75 column. An amount of eluent equal to 10 mL was collected in each tube, and the absorbance at 490 nm was measured. The fractions (SUSP-4) were then processed.

2.3. Characterization of SUSP-4

2.3.1. High-performance gel permeation chromatography (HPGPC)

SUSP-4 and standard were weighed and prepared as 5 mg/mL solutions, and the supernatant was filtered by 0.22-μm microporous filter membrane for the assay. The chromatographic column was a BRT105-104-102 tandem gel column (8 mm × 300 mm) with an RI-10A differential detector (Shimadzu, Kyoto, Japan). The column temperature was set at 40 °C. The mobile phase (0.6 mL/min) was 0.05 M NaCl solution. The injection volume was 20 μL.

2.3.2. Fourier transform infrared (FT-IR) spectroscopy

SUSP-4 (2 mg) and potassium bromide (200 mg) were mixed and pressed into tablets. The blank control was made from potassium bromide powder, which was scanned and recorded by FT-IR 650 (Tianjin Gangdong Sci. & Tech. Co., Ltd., Tianjin, China).

2.3.3. Monosaccharide composition

A 3 M TFA (10 mL) solution was added to 10 mg of SUSP-4 in an ampoule, which was processed at 120 °C for 3 h. The acid hydrolyzed solution was mixed by vortexing with 10 mL of water. One hundred microliters of the solution were aspirated, and purified water (0.9 mL) was added and centrifuged (12,000 rpm, 5 min) for ion chromatography (Thermo Fisher Scientific Inc., Waltham, MA, USA) analysis. A Dionex-Carbopac™ PA20 column (3 mm × 150 mm) and electrochemical detector (Ultimate™ 3000; Thermo Fisher Scientific Inc.) were used. The column temperature and injection volume were set at 30 °C and 5 μL. The mobile phases at 0.3 mL/min was composed of A (H_2O), B (15 mM NaOH), and C (15 mM NaOH and 100 mM NaOAC).

2.3.4. Glyoxalate reduction experiment

The reduction experiment was carried out by using a glyoxylate reducer. Distilled water and aldehyde activator were added to 80 mg of SUSP-4. The pH value was set at 4.6, and the reaction was performed for 3 h. Then, the pH value was set to 6.8, and the process was performed for 2 h. The sample was dialyzed in dialysis bags (1,000 Da), and the obtained sample was used for monosaccharide composition verification and subsequent methylation experiments.

2.3.5. Methylation analysis

The methylation assay was performed according to the kit (Borui Saccharide Biotech Co., Ltd., Yangzhou, China). After reduction with NaBD4, SUSP-4 (10 mg) was dialyzed and freeze-dried. Dimethyl sulfoxide (DMSO) was used to dissolve the dried sample, solid NaOH was added, and CH_3I was used to perform the methylation reaction. TFA (2 M) was used in the reaction process to produce the methylation product at 121 °C for 90 min. In the final step, 1 M NaBD4 was used to reduce the sample, and acetic anhydride was used to acetylate it. The instrument used for the study was a Shimadzu GC–MS-QP 2010 with RXI-5 SIL MS column (30 mm × 0.25 mm, 0.25 μm).

The carrier gas was helium (1 mL/min). The temperature program was set at 120 °C and then increased to 250 °C (3 °C/min) for 5 min. The inlet temperature was set at 250 °C.

2.3.6. Nuclear magnetic resonance (NMR) assay

A total of 50 mg of SUSP-4 was dissolved in 0.5 mL of deuterium oxide, freeze-dried, and redissolved in 0.5 mL of deuterium oxide.

The process was repeated. 1D and 2D NMR spectra were determined by a 600 MHz NMR instrument (Bruker, Billerica, MA, USA).

2.3.7. Rheological properties test

SUSP-4 was dissolved in purified water (1.5 mg/mL). A Discover HR-10 rheometer (TA Instruments, Newcastle, DE, USA) was used with an experimental temperature accuracy of ±0.1 °C. A parallel steel plate with a diameter of 60 mm and a gap of 1,000 μm between the upper and lower plates was used. For each measurement, a certain amount of sample was transferred and incubated on the plate for 3 min at 25 °C. An investigation of the sample's viscosity was conducted using a static rheology test. A temperature of 25 °C was used, and the range of shear rate scanning was 0.01–100 s^{-1}. The dynamic rheological test was performed in oscillation amplitude mode at 25 °C, a fixed oscillation frequency of 1 s, and a stress range of 0.1%–100.0%. The oscillation frequency mode was used to explore the variation pattern of the energy storage modulus (G′) and energy dissipation modulus (G″) of the tested sample. The stress was set in the linear viscoelastic interval, the frequency was 0.1–100 Hz, and the temperature was 25 °C (Discover HR-10, TA Instruments).

2.3.8. Atomic force microscopy (AFM)

SUSP-4 dissolved in 70% ethanol (20 μg/mL) was placed on a shaker, and shaken for 120 min (water bath at 60 °C). The solution (10 μL) was placed on mica sheets and dried at 25 °C for 12 h. Finally, an AFM (Dimension ICON, Bruker) scan was performed at 25 °C in knockdown mode with a scan range of 5 μm × 5 μm.

2.3.9. Transmission electron microscopy (TEM) analysis

SUSP-4 (1 mg/mL in water) solution was centrifuged. The prepared SUSP-4 was then added dropwise to the surface of the copper wire, and the droplets on the surface of the copper wire were dried with a tungsten lamp. The sample was observed under transmission electron microscope (HT7650; Hitachi, Tokyo, Japan) at room temperature (accelerating voltage: 80 kV).

2.4. Activity evaluation of SUSP-4

2.4.1. Animal experiments

Male C57BL/6J mice (18–22 g) were purchased from the Experimental Animal Center of Dalian Medical University (SCXK: 2020–0001). All animal care and laboratory procedures were carried out in accordance with the relevant regulations of the National Research Council's Guide for the Care and Use of Laboratory Animals and approved by the Animal Care and Use Committee of Dalian Medical University (Approval No.: AEE20046). All animals were kept in a controlled environment with a 12-h light schedule, constant temperature (20 ± 3 °C), and relative humidity (60% ± 10%). The mice were randomly divided into Control, Model, and SUSP-4 administration groups (50 and 100 mg/kg) after seven days of acclimatization feeding. The mice in Control group were given normal drinking water, and other animals were given 2.5% dextran sulfate sodium salt (DSS) solution for one week and then replaced with normal drinking water for one week. The process was repeated for three cycles. From the first day of modeling, the mice in the SUSP-4 groups were given 50 and 100 mg/kg doses of SUSP-4 by gavage daily, and the mice in Control and Model groups were given equal amounts of purified water. The body weights of mice were measured daily, and disease activity index (DAI) in the last cycle was recorded.

2.4.2. Determination of cytokines in serum

Myeloperoxidase (MPO), malondialdehyde (MDA), total superoxide dismutase (T-SOD), and catalase (CAT) in serum were measured using commercial kits (Nanjing Jiancheng Bioengineering Institute, Nanjing, China), and the levels of interleukin-1β (IL-Iβ), IL-6, and tumor necrosis factor-α (TNF-α) in serum were measured by enzyme-linked immunosorbent assay (ELISA) kits (Meibiao Biotechnology, Jiangsu, China).

2.4.3. Histopathological examination

The colon tissues of the animals were rapidly dissected and collected, fixed with 4% paraformaldehyde at 4 °C, and then embedded in paraffin. Sections were stained with hematoxylin and eosin (H&E).

2.4.4. Immunofluorescence assay

After deparaffinization, the sections were incubated with antibodies against ZO-1 and occludin (1:50 dilution) at 4 °C. The next day, the sections were washed 3 times, and then the labeled secondary antibody (1:500, dilution) was added and incubated for 1 h. After incubation with 4',6-diamidino-2-phenylindole (DAPI) (1:100, dilution), the samples were photographed under an inverted fluorescence microscope (TE2000U; Nikon, Tokyo, Japan).

2.4.5. Western blotting assay

After sodium dodecyl sulfate-polyacrylamide gel electrophoresis (SDS-PAGE) electrophoresis, membrane transfer, and antibody incubation, enhanced chemiluminescence was used to check protein expression. Please refer to the Supplementary data for more details.

2.4.6. Fecal microbiota transplantation (FMT)

FMT experiments were performed as previously reported [22]. Prior to the transplantation experiment, recipient mice were subjected to triple antibiotic gavage (vancomycin 0.5 mg/mL, ampicillin 1 mg/mL, and metronidazole 1 mg/mL) for three days. The donor mice were divided into Control, SUSP-4, Model, and Model + SUSP-4 groups. Thirty-two mice in recipient group were randomly assigned to the Control-DSS, Model-DSS, SUSP-4-DSS, and SUSP-4 + Model-DSS groups. The IBD Model was established, and 100 μL of fresh bacterial suspension was administered by gavage every two days. The body weights were recorded before transplantation, and the DAI index at the last cycle was recorded. Then, colon tissue tests, immunofluorescence staining, serum index detection, and Western blotting assays were carried out.

2.4.7. 16S ribosomal RNA (rRNA) sequencing

After extracting the total genomic DNA from the sample, different regions of the gene are amplified using specific primers and barcodes. Refer to the Supplementary data for more details.

2.4.8. Untargeted metabolomics analysis

Untargeted metabolomics was performed using ultra-high performance liquid chromatography-tandem mass spectrometry (UHPLC-MS/MS) [23] and gas chromatography time-of-flight mass spectrometry (GC-TOF-MS) [24,25]. Please refer to the Supplementary data for detailed methods and chromatographic conditions (Tables S1 and S2).

2.4.9. Targeted metabolomics analysis of B vitamins

Absolute quantification of B vitamins in mouse feces was performed by UHPLC-MS/MS targeted metabolomics [26]. Sample processing and chromatographic conditions are provided in the Supplementary data.

2.4.10. Cell culture and treatment

RAW264.7 cells were cultured in Dulbecco's modified eagle medium (Procell, Wuhan, China) supplemented with D-glucose (4.5 g/L), 1% penicillin-streptomycin and 10% fetal bovine serum

(FBS) at 37 °C in 5% CO_2 condition. The concentrations of SUSP-4 and LPS were carried out with the reports [27,28]. The cells inoculated in 6-well plates were treated and LPS (0.5 μg/mL) was used directly for 24 h to induce M1 macrophages. These cells were divided into Control, Model, 100 μg/mL SUSP-4, 200 μg/mL SUSP-4, and 10 μM THA groups. Then, the protein levels of CD68 and CD86 were detected.

2.5. Statistical analysis

Origin 2018 software was used to draw HPGPC, ion chromatography (IC), and GC-MS figures of the structural characterization. SPSS 20.0 and GraphPad were used to analyze anti-IBD activity data by one-way analysis of variance (ANOVA). All data were evaluated as the mean ± standard deviation (SD). $^{*}P < 0.05$ and $^{**}P < 0.01$ were defined as significant differences.

3. Results

3.1. The acquisition of SUSP-4

A crude polysaccharide with a yield of 3.5% ± 0.3% from *S. uncinata* was obtained. Based on the elucidation curve (Fig. 1A), four fractions of the DEAE-52 cellulose column were produced. The part eluted by 0.3 M NaCl solution was further purified using a Sephadex G-75 column (Fig. 1B). In the end, SUSP-4 was produced as a light-yellow powder with a yield of 0.27% ± 0.06%.

3.2. Purity and molecular weight of SUSP-4

HPGPC showed a single peak with a stable and symmetrical baseline (Fig. 1C), demonstrating that SUSP-4 was pure polysaccharide. The heavy average molecular weight (M_w) was calculated to be 48,044 Da, and the number average molecular (M_n) and dispersity (M_w/M_n) were 32,477 Da and 1.48, respectively.

3.3. FT-IR of SUSP-4

In Fig. 1D, the stretching vibration of −OH was 3,600−3,200 cm^{-1} and the stretching vibration of O−H was 3,397 cm^{-1}, which are the characteristic peaks of sugars. Stretching vibrations of C−H were 2,923 and 2,854 cm^{-1}, and 1,610 cm^{-1} was water crystallization. Stretching vibration of C=O was 1720 cm^{-1}. 1411, 1,240, 1,141, and 1,099 cm^{-1} were stretching vibrations of C−O. 1,332 cm^{-1} was symmetric stretching vibration of C=O. 1,018 cm^{-1} was variable angle vibration of O−H. 956 cm^{-1} was the transverse rocking vibration of the terminal hypo methyl group of the pyran ring. 917 cm^{-1} was the asymmetric ring stretching vibration of the pyran ring. 894 cm^{-1} was variable angle vibration of C−H of the β-end group differential isomerism of the pyran ring.

3.4. Monosaccharide composition of SUSP-4

The composition of SUSP-4 is shown and listed in Fig. 1E and Table 1. SUSP-4 was composed of galacturonic acid (37.3%), galactose (16.5%), arabinose (13.8%), rhamnose (11.7%), and xylose (7.3%), with a molar ratio of 1.60:1.89:2.26:1.00:5.11, respectively. The presence of acidic groups caused it to become less susceptible to gasification and hydrolysis. Therefore, the acidic group of SUSP-4 was reduced before the methylation experiment (Fig. 1F and Table 2). After reduction, the main monosaccharide composition was rhamnose (8%), arabinose (8.5%), galactose (52.9%), and xylose (6.9%), with a molar ratio of 1.16:1.23:7.67:1.00.

3.5. Type of glycosidic bond of SUSP-4

In Fig. 1G and Table 3, Araf-1-5 (8.39%), Xylp-1-4 (4.71%), Galp-1 (5.41%), Rhap-1-2-4 (3.41%), Galp-1-6 (5.25%), Galp-1-4 (35.62%), Glcp-1-4 (6.72%), and Galp-1-3-4 (11.84%) were the major glycosidic bonds of SUSP-4. The secondary mass spectra are shown in Fig. S1.

3.6. NMR characteristics of SUSP-4

^{1}H NMR spectrum (Fig. 2A) signals were concentrated mainly between 3.0 and 6.0 ppm. Peaks between 3.2 and 4.0 ppm corresponded to sugar ring protons. The end-base proton peaks were concentrated at 4.3−6.0 ppm, and the main signal peaks were 5.16, 5.11, 5.05, 5.01, 4.98, 4.84, 4.51, 4.38, and 4.35 ppm. ^{13}C NMR spectrum (Fig. 2B) signals were concentrated mainly between 60 and 120 ppm. The anomeric carbon regions were mainly between 93 and 120 ppm, which were 108.8, 107.8, 104.9, 104.5, 103.0, 101.4, 100.4, and 99.8 ppm. The other main signal peaks were at 60−85 ppm. The Dept-135 spectrum (Fig. 2C) revealed four inverted peaks at 68.3, 64.3, 64.0, and 62.3 ppm, indicating the signal peaks of the pyran ring C6 or C5 [29,30]. In the heteronuclear single-quantum correlation spectrum (Fig. 2D), the anomeric hydrogen signal was 5.05 ppm, and the corresponding carbon signal was 108.8 ppm. By observing the ^{1}H-^{1}H correlated spectroscopy (COSY) spectrum (Fig. 2E), the signals of H1-2, H2-3, H3-4, and H4-5a were 5.05/4.07 ppm, 4.07/3.94 ppm, 3.94/4.15 ppm, and 4.15/3.81 ppm, respectively. We confirmed that H1, H2, H3, H4, and H5a were 5.05, 4.07, 3.94, 4.15, and 3.81 ppm, respectively, and the corresponding C1−C5 were 108.9, 82.2, 78.1, 83.7, and 68.3 ppm. Therefore, the signal should be attributed to →5)-α-L-Araf-(1→ . Therefore, this confirms that the signal was →5)-α-L-Araf-(1→ . Based on similar patterns and combining heteronuclear multiple bond correlation (HMBC) and nuclear overhauser effect spectroscopy (NOESY) spectra (Figs. 2F and G), all glycosidic bond signals were confirmed. These results are listed in Table 4 and in previous studies [9,31,32]. In the NOESY spectrum, the anomeric hydrogen of →5)-α-L-Araf-(1→ and H5 of →2,5)-α-L-Araf-(1→ indicated the presence of →5)-α-L-Araf-(1→2,5)-α-L-Araf-(1→ .

The presence of correlation peaks between α-L-Araf-(1→ anomeric hydrogen and H2 of →2,5)-α-L-Araf-(1→ indicated the presence of α-L-Araf-(1 → 2,5)-α-L-Araf-(1→ . The peaks between →2,5)-α-L-Araf-(1→ anomeric hydrogen and H4 of →2,4)-α-L-Rha-(1→ showed the presence of →2,5)-α-L-Araf-(1 → 2,4)-α-L-Rha-(1→ . The anomeric hydrogen of →6)-β-D-Galp-(1→ with the peak at H4 of →4)-α-D-GalAp-(1→ indicated the presence of →6)-β-D-Galp-(1→4)-α-D-GalAp-(1→ . The anomeric hydrogen of β-D-Galp-(1→ with an H4 peak of →4)-β-D-Xylp-(1→ indicated the presence of β-D-Galp-(1→4)-β-D-Xylp-(1→. The anomeric hydrogen of →4)-β-D-Xylp-(1→ with the H3 peak of →3,4)-α-D-GalAp-(1→ showed the presence of →4)-β-D-Xylp-(1→3,4)-α-D-GalAp-(1→. The anomeric hydrogen of →4)-α-D-GalAp-(1→ showed a peak with H4, indicating the presence of →4)-α-D-GalAp-(1→4)-α-D-GalAp-(1→. The anomeric hydrogen of →4)-α-D-GalAp-(1→ had a correlation peak with H-4 of →3,4)-α-D-GalAp-(1→, indicating the presence of →4)-α-D-GalAp-(1→3,4)-α-D-GalAp-(1→ . The anomeric hydrogen of →3,4)-α-D-GalAp-(1→ was a peak with H2 of →2,4)-α-L-Rha-(1→, suggesting the presence of →3,4)-α-D-GalAp-(1→2,4)-α-L-Rha-(1→ .

The structure of SUSP-4 is shown in Fig. 2H. The main chain of the structure was →6)-β-D-Galp-(1→4)-α-D-GalAp-(1→2)-α-L-Rha-(1→, while the branched β-D-Galp-(1→4)-β-D-Xylp-(1→ and →5)-α-L-Araf-(1→2,5)-α-L-Araf-(1→ by →3,4)-α-D-GalAp-(1→ and →2,4)-α-L-Rha-(1→ with O-3 and O-4 attached to the backbone.

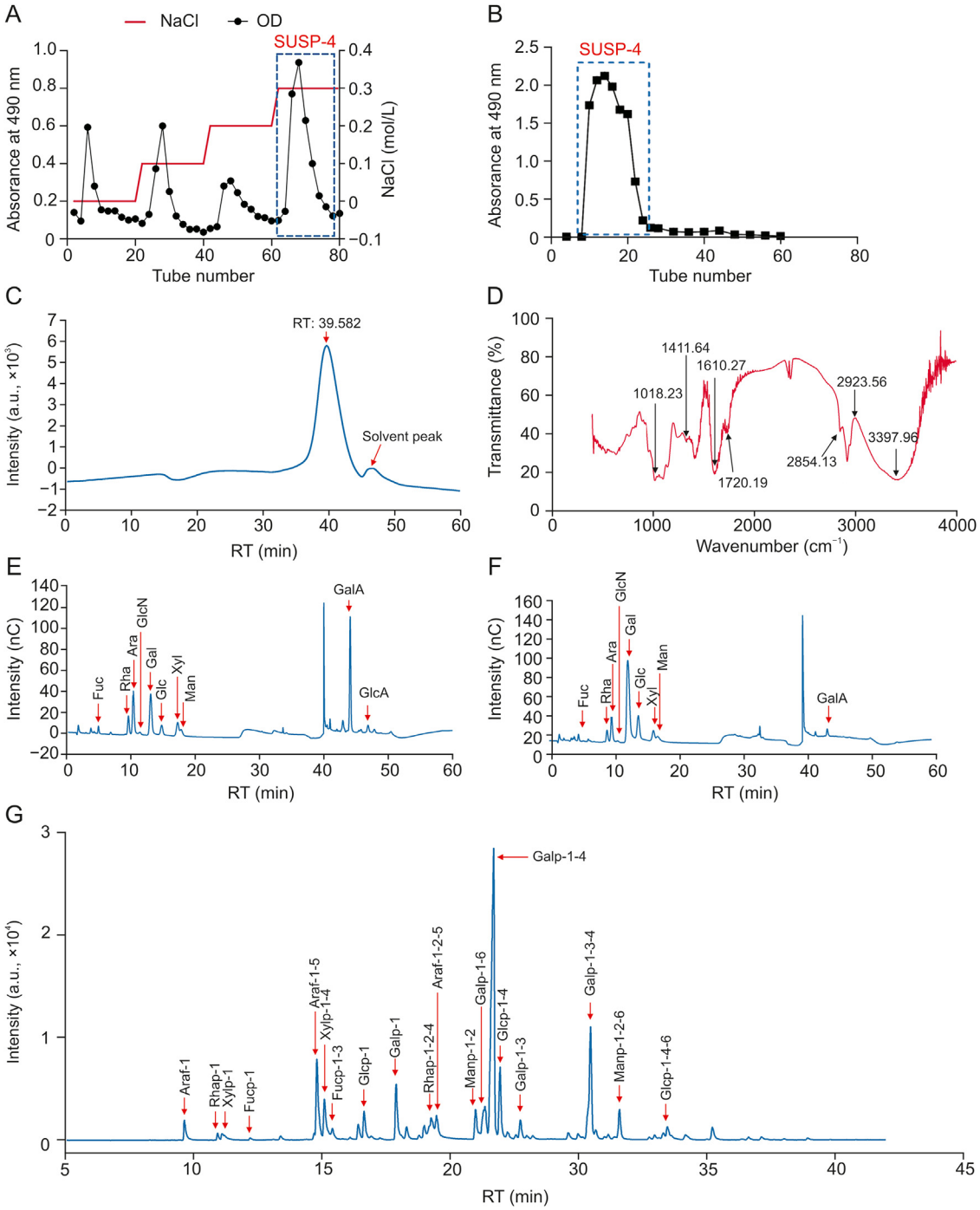

Fig. 1. Acquisition and structural characterization of SUSP-4. (A) Elution profile of SUSP on a DEAE-cellulose-52 column. (B) Elution profile of SUSP-4 on a Sephadex-G75 column. (C) High-performance gel permeation chromatography (HPGPC) chromatogram of SUSP-4. (D) Fourier transform infrared (FT-IR) spectrum of SUSP-4. (E) Ion chromatogram of monosaccharide compositions of SUSP-4. (F) Reduced monosaccharide composition of SUSP-4. (G) Gas chromatography-mass spectrometry (GC-MS) chromatogram of methylation analysis of SUSP-4. OD: optical density; RT: retention time; nC: nano Coulomb.

3.7. Flow behavior of SUSP-4

In Fig. 3A, the apparent viscosity gradually decreased with increasing shear rate, suggesting that the pseudoplastic fluid in the non-Newtonian fluids of SUSP-4 thinned under shear. The energy storage modulus G′ refers to the capacity of viscoelastic materials to store energy in a cycle under the action of alternating stress, usually named elasticity. The energy loss modulus G″ is the capacity of energy consumed in a change cycle, usually referred to as viscosity. In the linear viscoelastic region, the viscoelasticity of the sample was obtained by changing the frequency. The results in Fig. 3B showed that G′ was greater than G″, indicating that SUSP-4 exhibited rheological behavior with elasticity greater than viscosity.

3.8. AFM characteristics of SUSP-4

The AFM results of the planar and 3D images of the sample are shown in Fig. 3C. Among them, SUSP-4 showed a heterogeneous

Table 1
Monosaccharide composition data of SUSP-4.

Name	Retention time (min)	Mole ratio	Area
Fucose	4.884	0.013	1.272
Amino galactose hydrochloride	9.117	0.000	0
Rhamnose	9.534	0.117	4.683
Arabinose	10.292	0.138	12.487
Glucosamine hydrochloride	11.309	0.003	0.595
Galactose	12.992	0.165	15.510
Glucose	14.692	0.039	3.571
N-acetyl-D-glucosamine	15.975	0.000	0
Xylose	17.175	0.073	5.823
Mannose	17.709	0.050	2.589
Fructose	20.609	0.000	0
Ribose	22.709	0.000	0
Galacturonic acid	43.967	0.373	23.651
Guluronic acid	44.375	0.000	0
Glucuronic acid	46.734	0.027	2.100
Mannuronic acid	49.067	0.000	0

Table 2
Composition data of monosaccharides after reduction of SUSP-4.

Name	Retention time (min)	Mole ratio	Area
Fucose	4.709	0.016	1.360
Aminogalactose hydrochloride	8.759	0.000	0
Rhamnose	9.167	0.080	3.420
Arabinose	9.892	0.085	7.940
Glucosamine hydrochloride	10.825	0.002	0.319
Galactose	12.409	0.529	44.066
Glucose	14.059	0.116	9.930
N-acetyl-D-glucosamine	15.275	0.000	0
Xylose	16.417	0.069	4.973
Mannose	17.075	0.064	3.292
Fructose	19.717	0.000	0
Ribose	21.825	0.000	0
Galacturonic acid	43.575	0.040	1.836
Guluronic acid	43.942	0.000	0
Glucuronic acid	45.834	0.000	0
Mannuronic acid	48.334	0.000	0

patchy structure, suggesting the presence of polysaccharide molecular aggregated and entangled molecules, which may originate from strong intra- and inter-molecular interactions formed with hydroxyl groups. The molecular single chain was generally 0.1–1.0 nm. The height of SUSP-4 was from −9.7 to 29.1 nm, suggesting that SUSP-4 was not a single sugar chain, and the multiple sugar chains entwined into strands.

3.9. TEM characteristics of SUSP-4

As shown in Fig. 3D, SUSP-4 dissolved in water showed a spherical shape with a relatively uniform particle size and good dispersion.

3.10. SUSP-4 significantly reduces the symptoms of IBD mice

Fig. 4A shows the body weight data. Fig. 4B shows the DAI scores of the mice. Compared with Model group, SUSP-4 at 100 mg/kg significantly improved body weight and DAI score. In Fig. 4C, the colon length in Model group was obviously shortened, which was obviously improved by SUSP-4.

3.11. Protective effect of SUSP-4 on colonic structures in IBD mice

In Fig. 4D, the mice in Control group had intact colonic morphology, intestinal mucosa, and U-shaped recess structure. The colon of mice in Model group was severely damaged, the arrangement of cup-shaped cells was disturbed, and the U-shaped crypt was damaged and infiltrated with massive inflammatory cells. These injuries were significantly ameliorated by SUSP-4. In Fig. 4E, the levels of occludin and ZO-1, the key proteins on the intestinal barrier, were markedly decreased in Model mice and were significantly increased by SUSP-4.

3.12. SUSP-4 reduces inflammatory and oxidative stress levels in IBD mice

In Fig. 4F, compared with Model group, SUSP-4 markedly attenuated the serum levels of MPO, MDA, IL-6, IL-1β, and TNF-α, and markedly upregulated the levels of CAT and T-SOD.

3.13. SUSP-4 regulates gut microbiota in IBD mice

In Fig. 5A, the closer sample distance indicated a more similar species composition structure based on the principal coordinates analysis (PCoA) model. The samples from Control, Model, and SUSP-4 group showed an overall homogeneous clustering pattern. In Fig. 5B, the number of common operational taxonomic unit sequences among the three groups was 596. Fig. 5C shows the level of gut

Table 3
Methylation analysis data of SUSP-4.

Retention time (min)	Methylated sugar	Mass fragments (*m/z*)	Area (%)	Type of linkage
9.623	2,3,5-Me3-Araf	43, 71, 87, 101, 117, 129, 145, and 161	1.80	Araf-1
10.915	2,3,4-Me3-Rhap	43, 72, 89, 101, 115, 117, 131, 161, and 175	0.48	Rhap-1
11.081	2,3,4-Me3-Xylp	43, 87, 101, 117, 131, 161, 173, 205	1.04	Xylp-1
12.196	2,3,4-Me3-Fucp	43, 72, 89, 101, 115, 117, 131, 161, and 175	0.21	Fucp-1
14.784	2,3-Me2-Araf	43, 87, 99, 101, 117, 129, and 189	8.39	Araf-1-5
15.076	2,3-Me2-Xylp	43, 87, 101, 117, 129, 161, and 189	4.71	Xylp-1-4
15.390	2,4-Me2-Fucp	43, 89, 101, 117, 131, 159, 173, and 233	1.23	Fucp-1-3
16.621	2,3,4,6-Me4-Glcp	43, 71, 87, 101, 117, 129, 145, 161, and 205	2.83	Glcp-1
17.871	2,3,4,6-Me4-Galp	43, 71, 87, 101, 117, 129, 145, 161, 205	5.41	Galp-1
19.233	3-Me1-Rhap	43, 87, 101, 117, 129, 143, 159, 189, and 203	3.41	Rhap-1-2-4
19.441	3-Me1-Araf	43, 85, 99, 117, 127, 131, 159, 201, and 261	2.35	Araf-1-2-5
20.964	3,4,6-Me3-Manp	43, 71, 87, 99, 101, 129, 145, 161, and 189	3.05	Manp-1-2
21.329	2,3,4-Me3-Galp	43, 71, 87, 99, 101, 117, 129, 161, 173, 189, and 233	5.25	Galp-1-6
21.666	2,3,6-Me3-Galp	43, 71, 87, 99, 101, 113, 117, 129, 131, 161, 173, and 233	35.62	Galp-1-4
21.923	2,3,6-Me3-Glcp	43, 71, 87, 99, 101, 113, 117, 129, 131, 161, 173, and 233	6.72	Glcp-1-4
22.710	2,4,6-Me3-Galp	43, 71, 87, 101, 117, 129, 161, 173, and 233	1.54	Galp-1-3
25.445	2,6-Me2-Galp	43, 87, 97, 117, 129, 143, 159, and 185	11.84	Galp-1-3-4
26.572	3,4–Me2-Manp	43, 87, 99, 113, 129, 173, 189, and 233	2.83	Manp-1-2-6
28.432	2,3-Me2-Glcp	43, 85, 99, 101, 117, 127, 142, 159, 201, and 261	1.29	Glcp-1-4-6

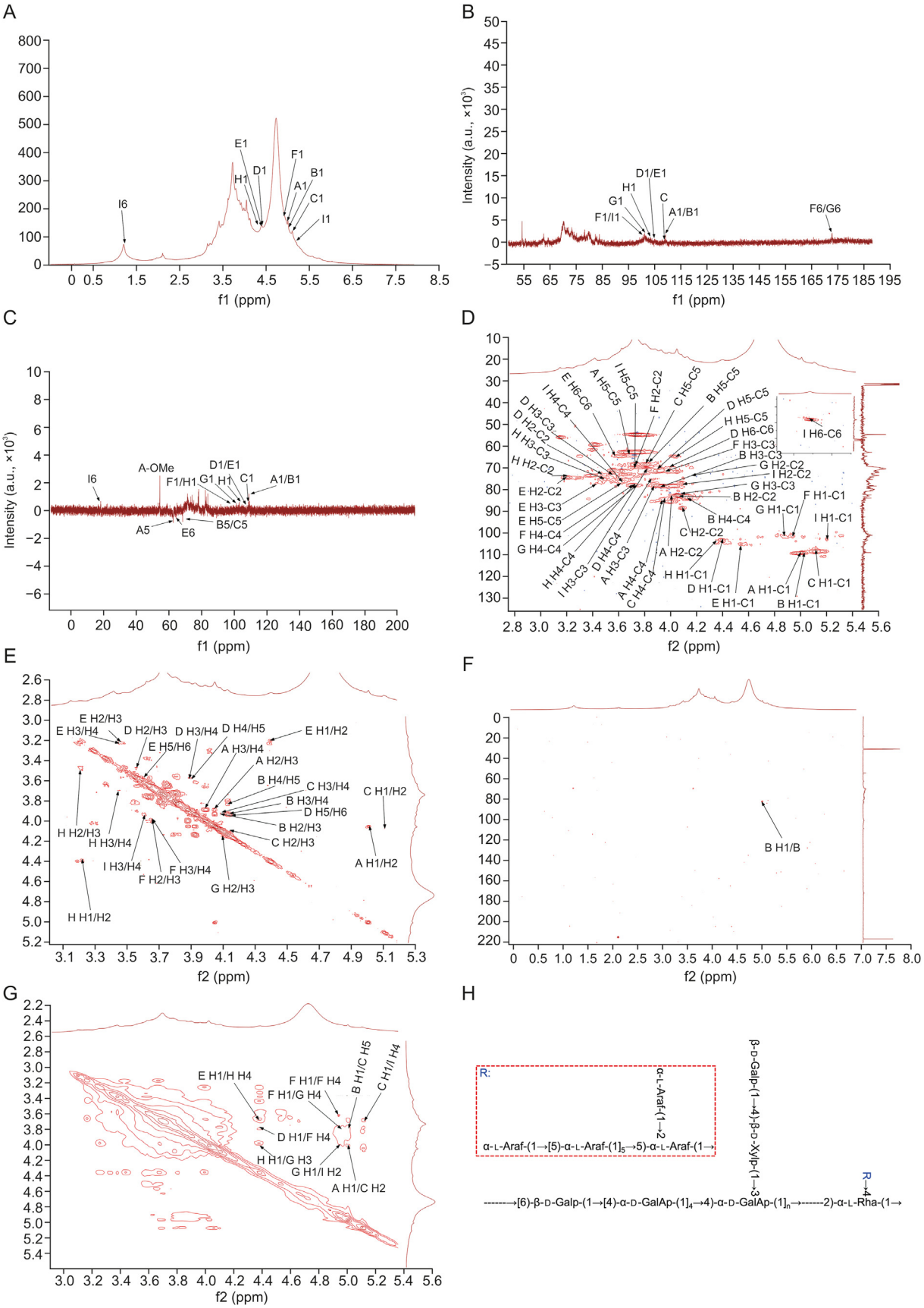

Fig. 2. Nuclear magnetic resonance (NMR) spectra of SUSP-4. (A) ^{1}H spectrum. (B) ^{13}C spectrum. (C) Dept-135 spectrum. (D) Heteronuclear single-quantum correlation spectrum. (E) ^{1}H-^{1}H correlated spectroscopy (COSY) spectrum. (F) Heteronuclear multiple bond correlation (HMBC) spectrum. (G) Nuclear overhauser effect spectroscopy (NOESY) spectrum. (H) Putative structure of SUSP-4. The "A–I" labeled in the diagram is the designation of the glycosidic bond. A: α-L-Araf-(1→; B: →5)-α-L-Araf-(1→; C: →2,5)-α-L-Araf-(1→; D: →6)-β-D-Galp-(1→; E: β-D-Galp-(1→; F: →4)-α-D-GalAp-(1→; G: →3,4)-α-D-GalAp-(1→; H: →4)-β-D-Xylp-(1→; and I: →2,4)-α-L-Rha-(1→. The detailed peaks information is listed in Table 4.

Table 4
Chemical shifts of resonances in ^{1}H nuclear magnetic resonance (NMR) and ^{13}C NMR of SUSP-4.

Signals	Glycosyl residues	H1/C1	H2/C2	H3/C3	H4/C4	H5/C5	C6/H6a,b	
A	α-L-Araf-(1→	5.01	4.01	3.84	3.92	3.70	3.37	
		108.80	82.70	77.80	85.10	62.30		
B	→5)-α-L-Araf-(1→	5.05	4.07	3.94	4.15	3.81	3.71	
		108.90	82.20	78.10	83.70	68.30		
C	→2,5)-α-L-Araf-(1→	5.11	4.09	4.19	3.94	3.81		
		107.80	88.50	78.30	83.80	68.30		
D	→6)-β-D-Galp-(1→	4.38	3.45	3.59	3.87	3.89	3.96	3.83
		104.90	72.20	73.90	75.00	69.90	70.50	
E	β-D-Galp-(1→	4.51	3.29	3.47	3.22	3.61	3.55	3.45
		104.50	74.70	76.60	83.40	77.40	64.00	
F	→4)-α-D-GalAp-(1→	4.98	3.68	3.94	3.68			3.73
		100.40	69.40	70.10	78.10	72.70	176.70	54.10
G	→3,4)-α-D-GalAp-(1→	4.84	4.18	4.10	3.67			
		101.40	72.70	82.60	78.10	71.80	176.70	
H	→4)-β-D-Xylp-(1→	4.35	3.23	3.50	3.71	4.04	3.32	
		103.00	74.00	75.00	77.70	64.30		
I	→2,4)-α-L-Rha-(1→	5.16	4.06	3.84	3.61	3.76	1.23	
		99.80	77.70	70.30	76.80	69.70	18.20	

microbiota between each sample and group (top 10). Fig. 5D shows the cluster analysis at genus, and Fig. 5E shows the differential genera regulated by SUSP-4. At the genus level, SUSP-4 significantly downregulated *Akkermansia* and *Alistipes*, increased *Muribaculaceae*, and decreased *Eubacterium coprostanoligenes* group compared with Model group. In Fig. 5F, the abundance of *Akkermansia* was increased at the phylum, class, order, family, and genus levels in Model group, which was markedly downregulated by SUSP-4.

3.14. SUSP-4 fecal transplantation alleviates symptoms in IBD mice

Fig. 6A shows the process of FMT experiment. Fig. 6B shows weight of mice, DAI scores, and area under the curve. The mice in SUSP-4-DSS and SUSP-4 + Model-DSS groups had less fluctuation in body weight and lower DAI scores, and the area under the curve was significantly reduced, indicating that the symptoms of IBD were improved compared with Model-DSS group. As shown in Fig. 6C, in Model-DSS group, the colon was markedly shortened and in SUSP-4-DSS and SUSP-4 + Model-DSS groups, the colon was significantly improved. In Fig. 6D, the colon damage was serious in Model-DSS group, and the pathological damage in the SUSP-4-DSS group was obviously improved. Although the SUSP-4 + Model-DSS group was improved, there was still massive inflammatory cell infiltration. In Fig. 6E, in Model-DSS group, immunofluorescence analysis indicated that occludin and ZO-1 expression levels were obviously decreased and were enhanced in SUSP-4-DSS and SUSP-4 + Model-DSS groups. The data in Fig. 6F show that compared with Model-DSS group, MPO, MDA, and three inflammatory factors in SUSP-4-DSS and SUSP-4 + Model-DSS groups were obviously downregulated, while the levels of CAT and T-SOD were markedly increased.

3.15. SUSP-4 regulates fecal metabolite levels in IBD mice

The results of untargeted metabolomics were based on the results of UHPLC-MS/MS and GC-TOF/MS. Fig. 7A shows the results of principal component analysis (PCA). Different samples in Control, Model, and SUSP-4 groups showed a general trend of aggregation, indicating that the types and contents of metabolites in the samples were similar. In Fig. 7B, the results showed an aggregation trend among the samples in the same group, which proved that there were obvious differences in intestinal metabolites among Control, Model, and SUSP-4 groups. The results of the orthogonal partial least squares-discriminant analysis (OPLS-DA) permutation test showed that R^2Y ($\approx$1) values were 0.086 and 0.081, and Q^2 ($\geq$0.4) values were 1.04 and 0.54 in the two comparison groups, indicating that the interpretability and predictability of the data met the requirements of analysis. Fig. 7C shows the volcanic map analysis of differential metabolites, in which the significantly upregulated metabolites, downregulated metabolites, and nonsignificant metabolites are colored red, blue, and gray, respectively. Fig. 8A and Table S3 show cluster analysis of differential metabolites. Compared with Model group, SUSP-4 significantly decreased the contents of 4,5-dimethyloxazole, *n*-carbamoyl putrescine, 8,11,14-eicosatrienoic acid, and 4-guanidino-butanoic acid. The contents of 71 metabolites, such as thiamine and pyrimidine, were significantly increased. In Fig. 8B, in Control group compared to Model group, five metabolic pathways with the highest differential metabolite enrichment were vitamin B6 metabolism, thiamine metabolism, alpha-linoleic acid metabolism, linoleic acid metabolism, and valine, leucine, and isoleucine biosynthesis. In Model group compared to SUSP-4 group the metabolic pathways were taurine and hypotaurine metabolism, thiamine metabolism, ubiquinone and other terpenoid-quinone biosynthesis, and nicotinate and nicotinamide metabolism. It was obvious that thiamine metabolism was the common pathway between groups, and SUSP-4 played a role in regulating this pathway. Combined with cluster analysis and pathway enrichment analysis, four metabolites, i.e., thiamine, pyridoxal, pyridoxamine, and pyridoxine, were selected as the targeted metabolic objects (Fig. 8C).

3.16. Conjoint analysis of differentially abundant bacteria and metabolites

Fig. 9A and Table S4 shows the results of the combined analysis of bacteria and differential metabolites. The results suggested that thiamine was negatively correlated with *Akkermansia*. SUSP-4 was able to significantly decrease *Akkermansia* and elevate the content of thiamine compared with Model group. This correlation was consistent with the regulatory effect of SUSP-4 on *Akkermansia* and thiamine.

3.17. SUSP-4 significantly increased thiamine levels in IBD mice

The results of B vitamins targeted metabolomics were based on the results of UPLC-MS/MS. Fig. 9B shows the PCA of fecal vitamin B-targeted metabolism in mice. Figs. 9C and D and Table S5 show the clustering analysis and absolute content statistics of B vitamins detected in mouse feces. From the results, SUSP-4 significantly

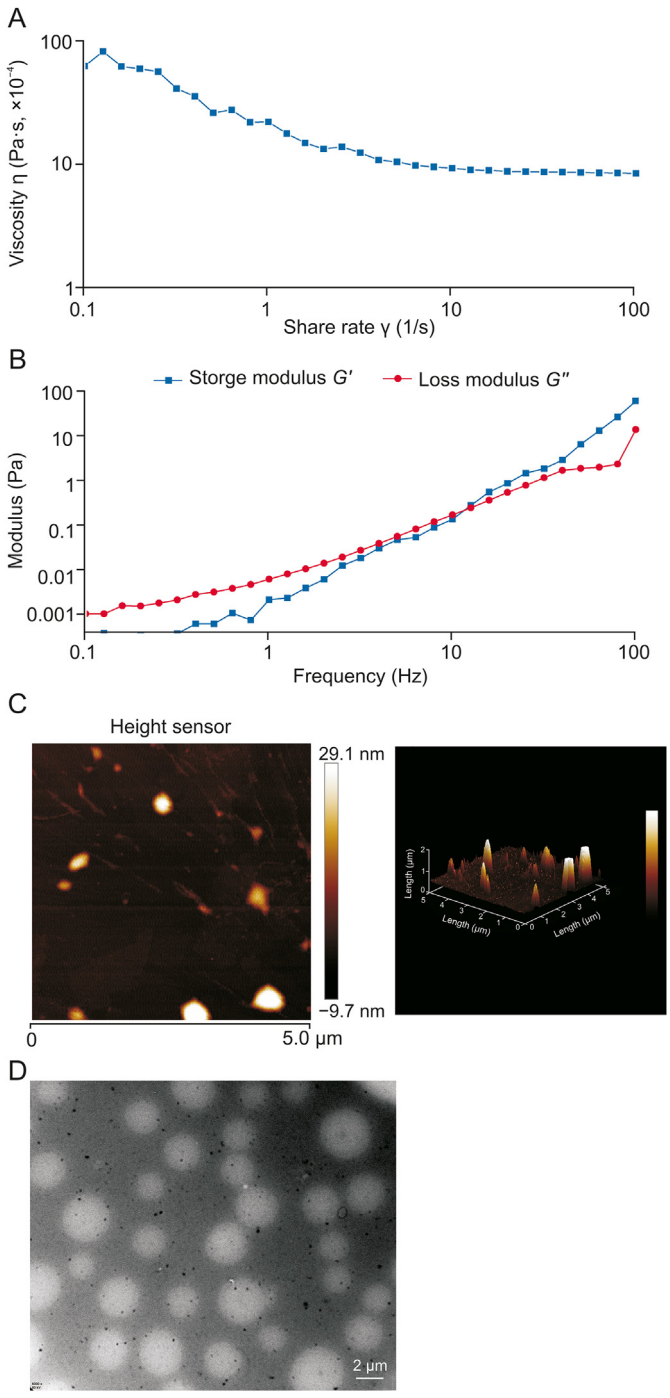

Fig. 3. Property analysis of SUSP-4. (A) Apparent viscosity of SUSP-4 relation curve with shear rate. (B) Relation curves between modulus energy storage modulus (G′) and energy dissipation modulus (G″) of SUSP-4 and oscillating strain. (C) Atomic force microscopy (AFM) characterization of SUSP-4. (D) Transmission electron microscope (TEM) analysis of SUSP-4.

elevated the thiamine content compared with Model group, which was consistent with the untargeted metabolomics assay.

3.18. SUSP-4 inhibits macrophage activation in IBD mice

In Figs. 10A–D, the results of immunofluorescence and Western blotting tests showed that CD68 and CD86 levels were obviously up-regulated in Model mice, which was reduced by SUSP-4, indicating that SUSP-4 inhibited the activation of macrophages on the colonic villi of mice. The same results were found in FMT test. The expression levels of CD68 and CD86 were significantly decreased in SUSP-4-DSS and SUSP-4 + Model-DSS groups.

3.19. Thiamine inhibits the activation of RAW264.7 macrophages

In Fig. 10E, compared with Model group, there were no significant changes in CD68 and CD86 levels in SUSP-4 group, but CD86 expression level in THA group was significantly decreased, indicating that thiamine effectively inhibited M1 polarization of macrophages.

3.20. SUSP-4 regulates NF-κB/Nrf2/COX-2 protein levels

In Fig. 11, SUSP-4 obviously increased Nrf2 and reduced COX-2 and p-NF-κB compared with Model group. In FMT experiment, Nrf2 in the SUSP-4-DSS and SUSP-4 + Model-DSS groups were markedly increased, and COX-2 and p-NF-κB were decreased compared with Model-DSS group.

4. Discussions

SUSP-4 polysaccharide from *S. uncinata* was purified by aqueous alcoholic precipitation and subsequently cellulose DEAE-52 and Sephadex G-75 gel column separation. The results of structural characterization experiments showed that SUSP-4 with a M_W of 48 kDa was composed mainly of galacturonic acid, galactose, arabinose, rhamnose, and xylose. The main types of glycosidic bonds were Araf-1-5, Galp-1-4, and Galp-1-3-4. The main chain composition of SUSP-4 was →6)-β-D-Galp-(1→4)-α-D-GalAp-(1→2)-α-L-Rha-(1→, while the branched chains β-D-Galp-(1→4)-β-D-Xylp-(1→ and →5)-α-L-Araf-(1→2,5)-α-L-Araf-(1→ were attached to O-3 and O-4 of →3,4)-α-D-GalAp-(1→ and →2,4)-α-L-Rha-(1→ . In the physicochemical property experiments, the elasticity of SUSP-4 was greater than its viscosity. The AFM results showed that SUSP-4 was not a single sugar chain, but multiple sugar chains entangled with each other to form chains. TEM features showed that the aqueous solution of SUSP-4 had good dispersion. It has been reported that galactose in polysaccharides may be associated with anti-inflammatory effects [33,34], and the galactose and galacturonic acid contained in SUSP-4 may be essential for this role.

IBD is the most common intestinal disease with symptoms of weight reduction, hematochezia, and diarrhea [35]. In this study, a mouse IBD Model was constructed by adding DSS to the drinking water via interval Modeling to simulate recurrent disease episodes. The DAI score demonstrated that SUSP-4 significantly improved the morbidity of IBD mice. Compared with Model group, mice in SUSP-4 group verified improvement in weight reduction, hematochezia, diarrhea, and shortened colon, and inflammation and oxidative stress in IBD were also reduced. The level of MPO associated with the severity of the disease has been reported to be markedly increased in IBD patients [36,37], and the results showed down-regulation in MPO levels after administration of SUSP-4. In addition, SUSP-4 improved the colonic mucosa, and the expression levels of two markers of the intestinal barrier (ZO-1 and occludin) were markedly increased, suggesting that SUSP-4 alleviated intestinal mucosal damage by reinforcing the intestinal barrier.

Polysaccharides act as a therapeutic agent for IBD by regulating intestinal flora [38]. In this work, 16S rRNA sequencing showed that SUSP-4 significantly decreased Verrucomicrobiota, Verrucomicrobae, and Verrucomicrobiales at the phylum, class, and order levels. At the family level, SUSP-4 significantly decreased Akkermansiaceae and increased Muribaculacea. At the genus level, it markedly decreased *Akkermansia* and *Alistipes* and increased the abundance of

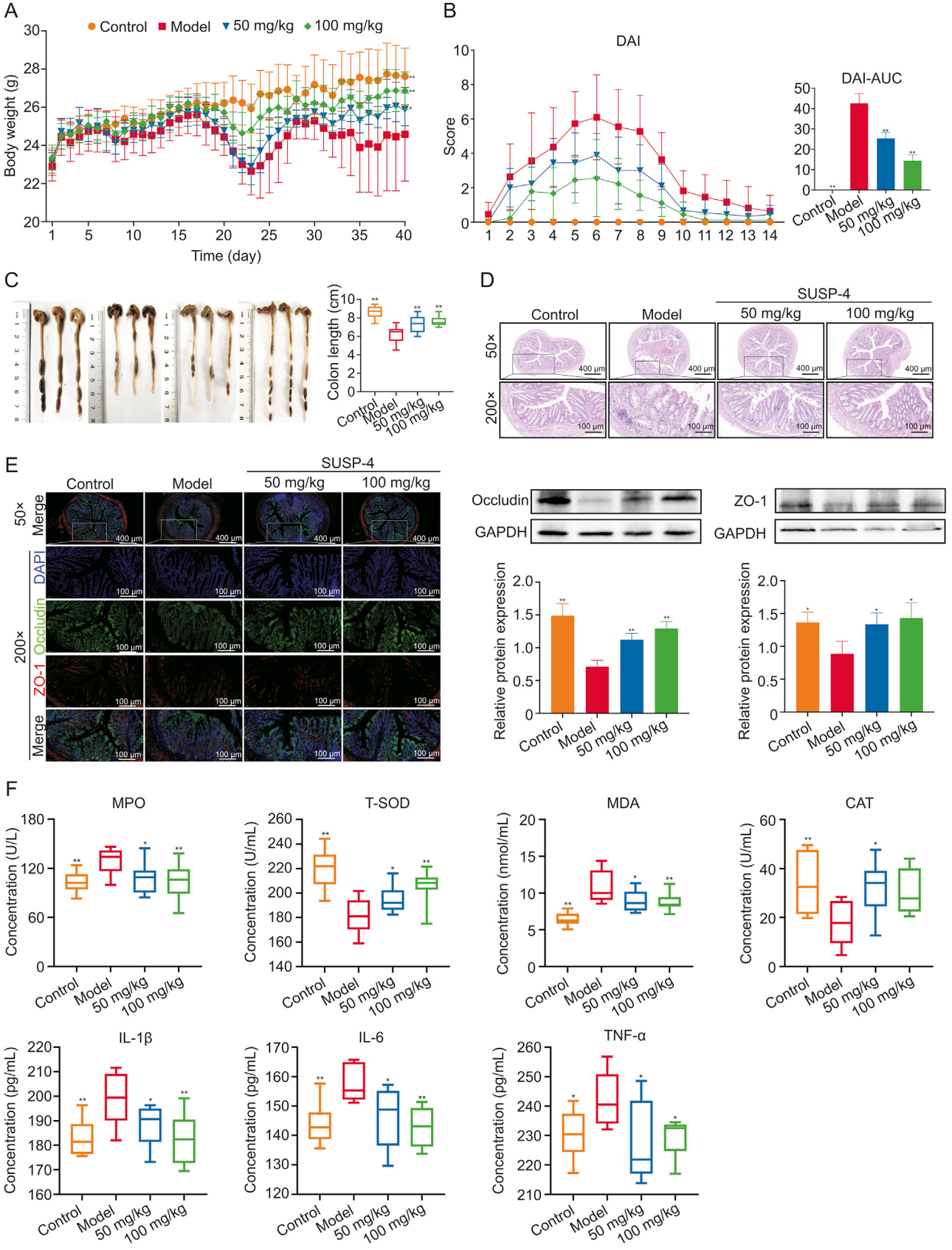

Fig. 4. SUSP-4 improves inflammatory bowel disease (IBD) symptoms in mice. (A) Experimental process diagram. (B) Body weight change and disease activity index (DAI) score in mice. (C) Colonic tissue measurement. (D) Hematoxylin-eosin (H&E) staining of colon. (E) Immunofluorescence staining of the colon and Western blotting assay. Red was zonula occludens protein 1 (ZO-1) and green was occludin. (F) Serum biochemical analysis of myeloperoxidase (MPO), malondialdehyde (MDA), total-superoxide dismutase (T-SOD), catalase (CAT), interleukin-1β (IL-Iβ), IL-6, and tumor necrosis factor-α (TNF-α). Data are presented as the mean ± standard deviation (SD) ($n = 8$). $^{*}P < 0.05$ and $^{**}P < 0.01$, compared with the Model group. AUC: area under the curve; DAPI: 4',6-diamidino-2-phenylindole; GAPDH: glyceraldehyde-3-phosphate dehydrogenase.

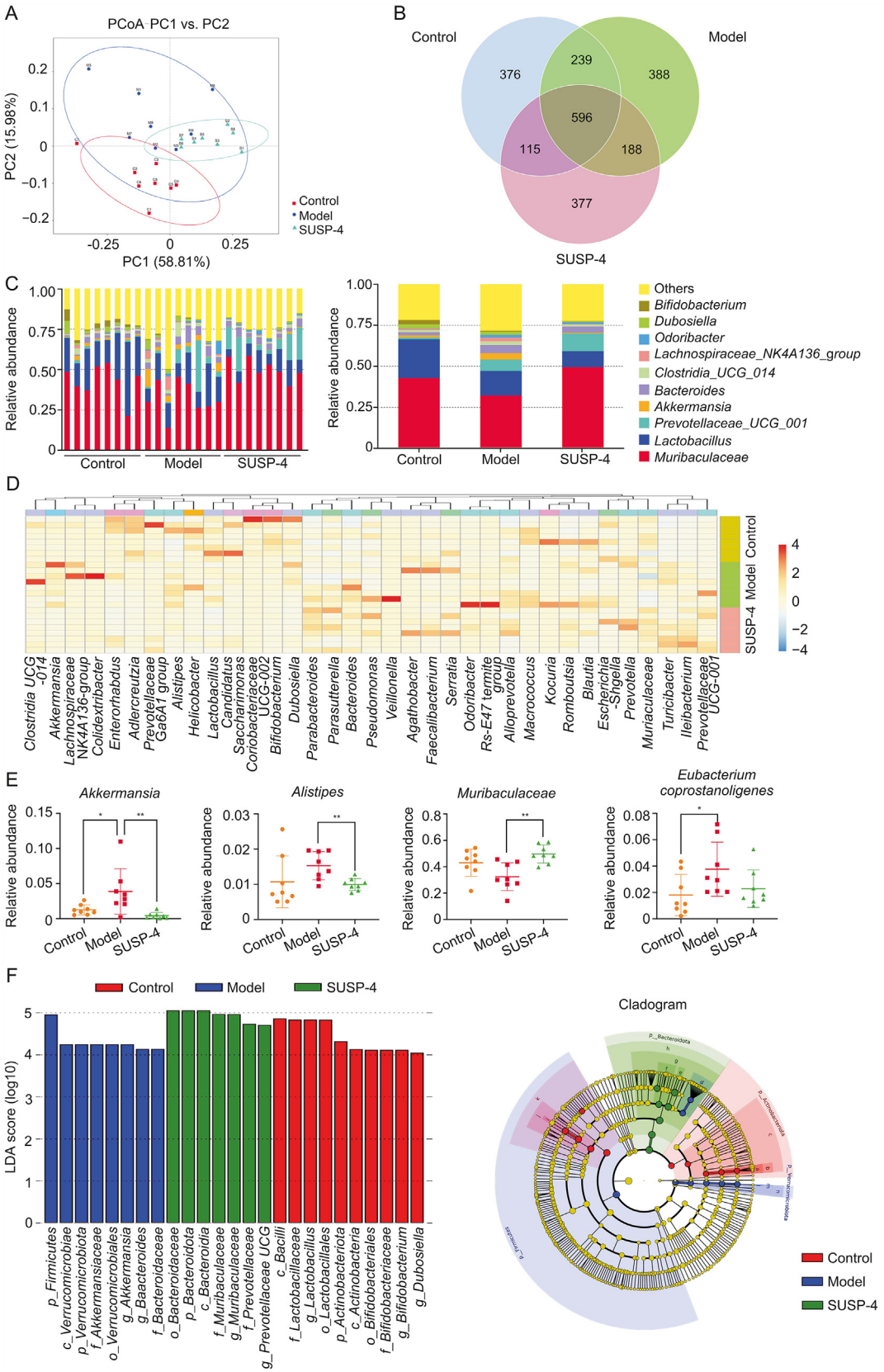

Fig. 5. 16S ribosomal RNA (rDNA) sequencing results. (A) Score scatter plot of the principal coordinates analysis (PCoA) model. (B) Venn graph. (C) Histogram of genus level abundance analysis. (D) Heatmap of hierarchical clustering analysis. (E) Differential bacteria analysis. (F) Linear discriminant analysis effect size. a: *f_Bifidobacteriaceae*; b: *o_Bifidobacteriales*; c: *c_Actinobacteria*; d: *f_Bacteroidaceae*; e: *f_Muribaculaceae*; f: *f_Prevotellaceae*; g: *o_ Bacteroidales*; h: *c_ Bacteroidia*; i: *f_Lactobacillaceae*; j: *o_Lactobacillales*; k: *c_Bacilli*; l: *f_Akkermansiaceae*; m: *o_ Verrucomicrobiales*; n : *c_Verrucomicrobiae*. Data are presented as the mean ± standard deviation (SD) ($n = 8$). $^{*}P < 0.05$ and $^{**}P < 0.01$, compared with the Model group. PC: principal component; LDA: linear discriminant analysis.

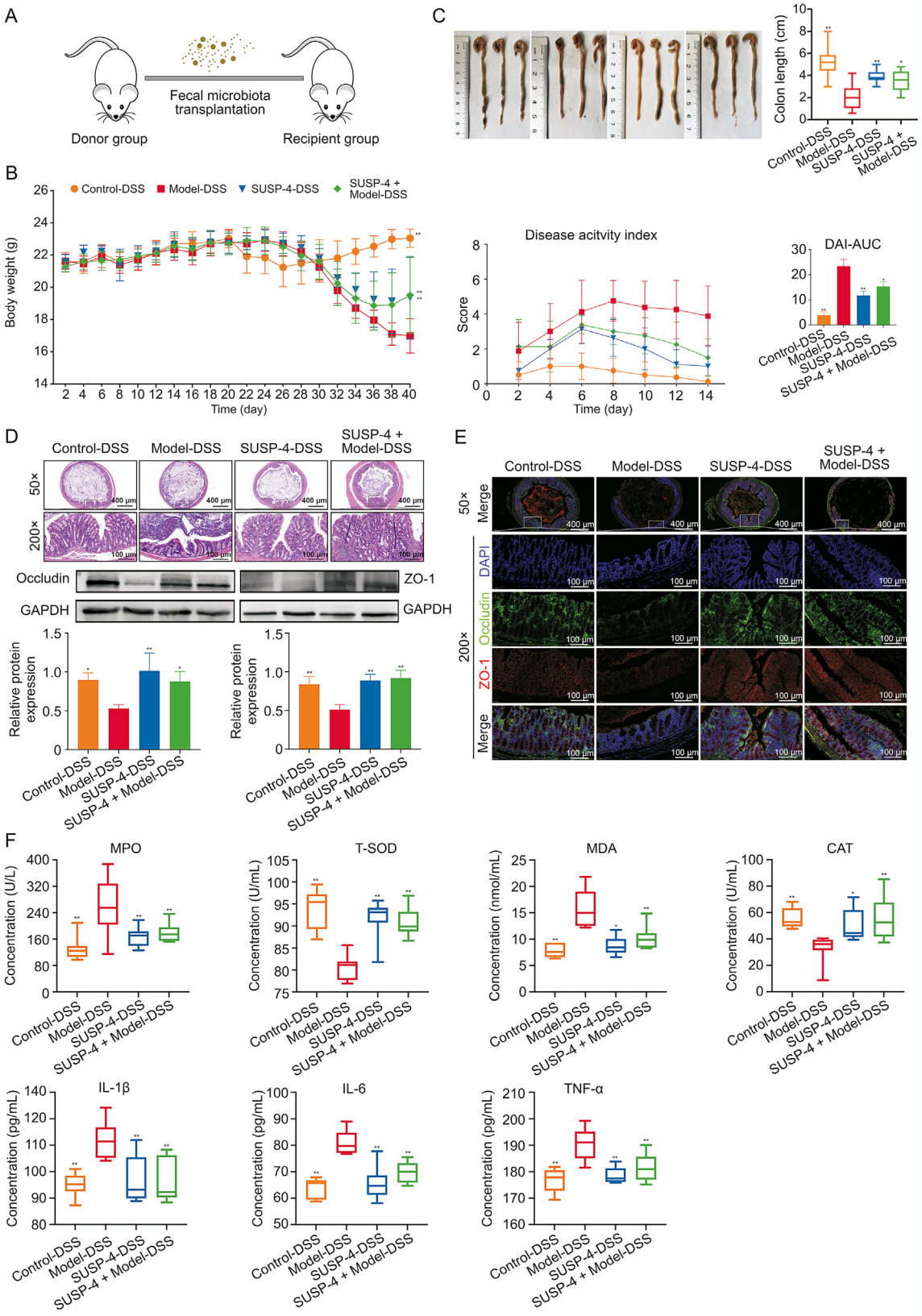

Fig. 6. SUSP-4 improved inflammatory bowel disease (IBD) symptoms in mice after fecal microbiota transplantation (FMT). (A) Experimental process diagram. (B) Body weight change and disease activity index (DAI) score. (C) Colonic tissue measurement. (D) Hematoxylin-eosin (H&E) staining of colon. (E) Immunofluorescence staining of the colon and Western blotting. Red is zonula occludens protein 1 (ZO-1) and green is occludin. (F) Serum biochemical analysis of myeloperoxidase (MPO), malondialdehyde (MDA), total-superoxide dismutase (T-SOD), catalase (CAT), interleukin-1β (IL-Iβ), IL-6, and tumor necrosis factor-α (TNF-α). Data are presented as the mean ± standard deviation (SD) ($n = 8$). $^{*}P < 0.05$ and $^{**}P < 0.01$, compared with Model-DSS group. DSS: dextran sulfate sodium; AUC: area under the curve; DAPI: 4',6-diamidino-2-phenylindole; GAPDH: glyceraldehyde-3-phosphate dehydrogenase.

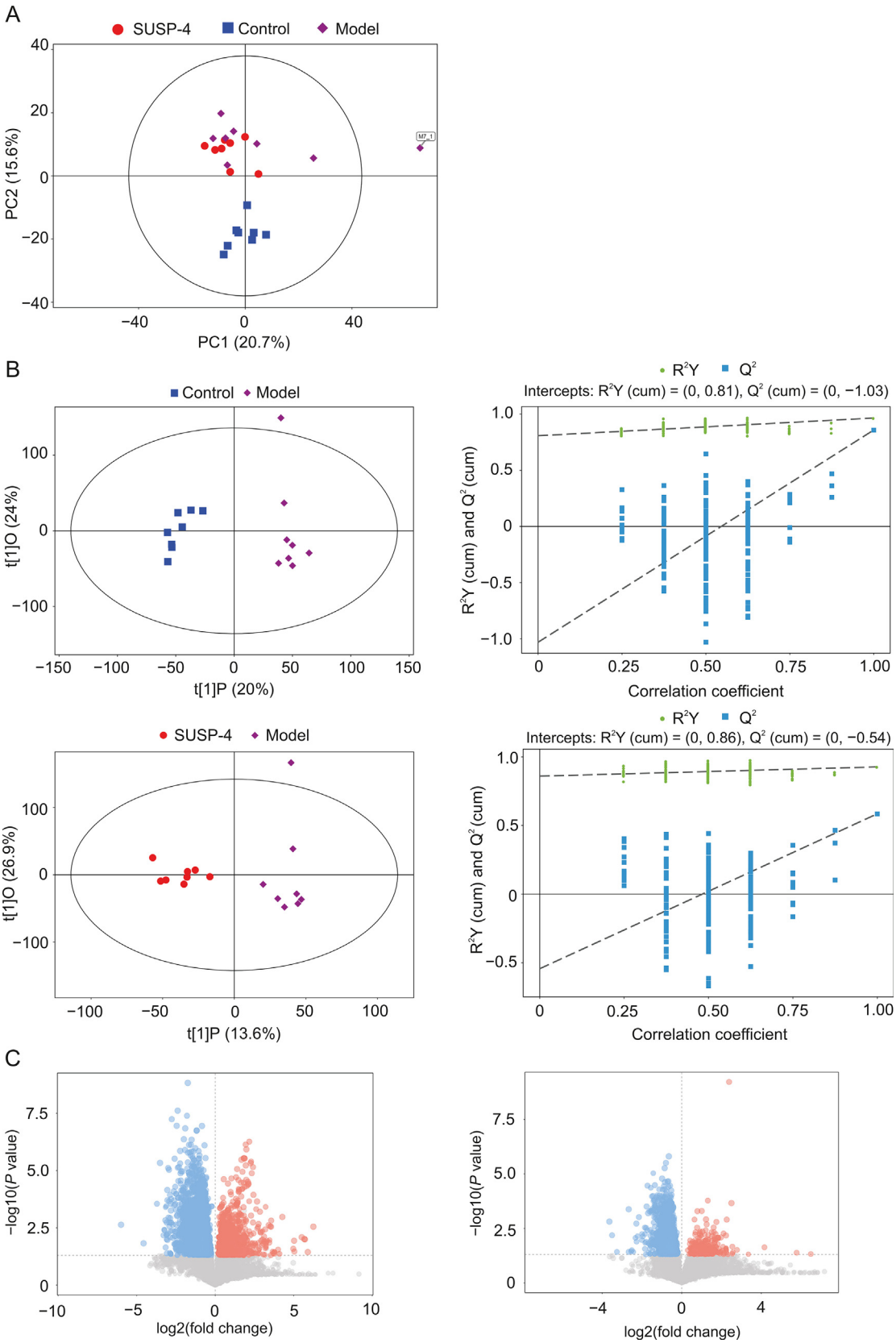

Fig. 7. Untargeted metabolomics analysis results. (A) Score scatter plot of the principal component analysis (PCA) model. (B) Score scatter plot and Permutation plot test of orthogonal partial least squares-discriminant analysis (OPLS-DA) for Model vs. Control and Model vs. SUSP-4. (C) Volcano plot for Model vs. Control and Model vs. SUSP-4. PC: principal component.

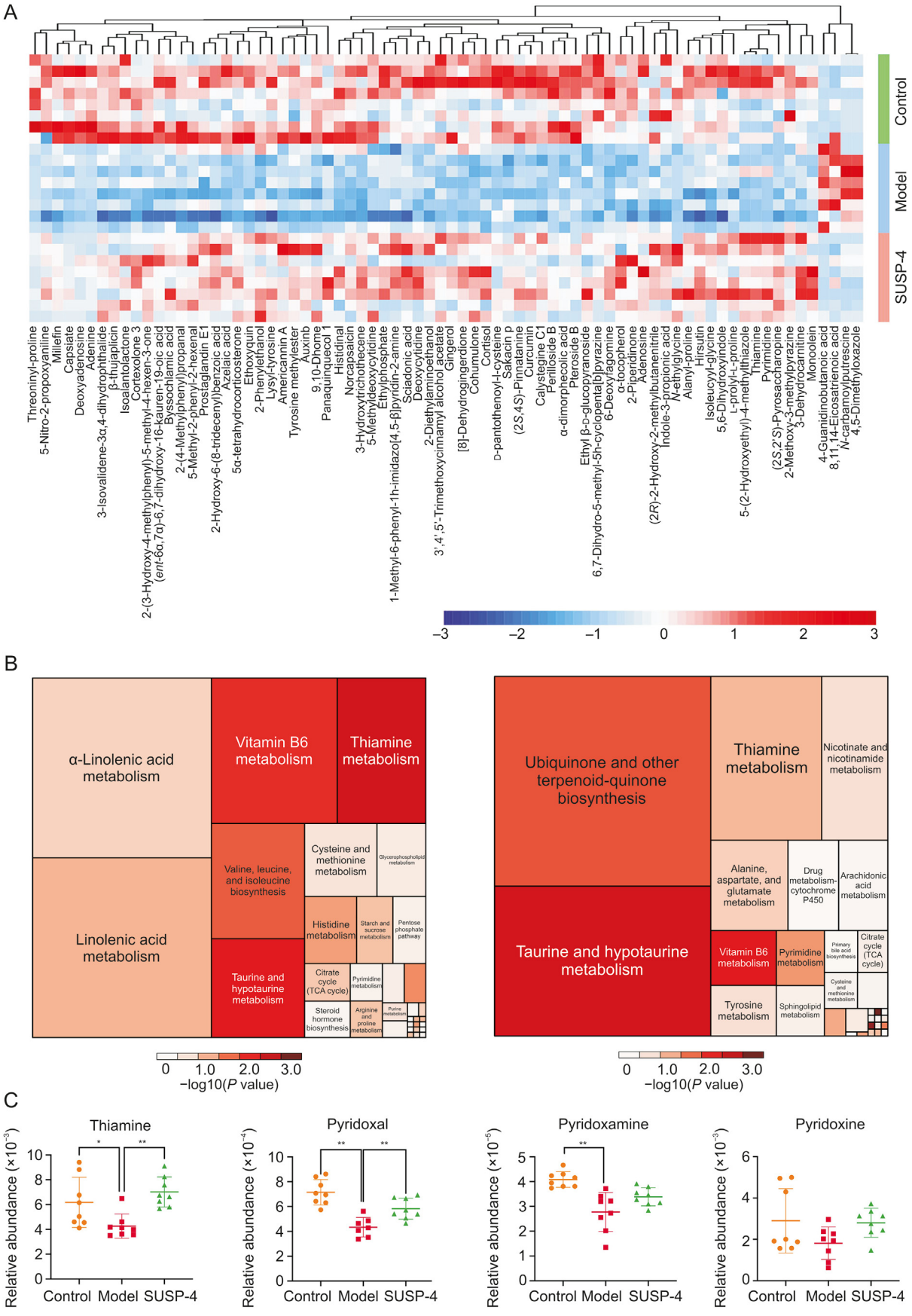

Fig. 8. Untargeted metabolomics statistics. (A) Heatmap of hierarchical clustering analysis. (B) Topology analysis of pathway analysis for Model vs. Control and Model vs. SUSP-4. (C) Differential metabolite analysis. Data are presented as the mean ± standard deviation (SD) ($n = 8$). $^{*}P < 0.05$ and $^{**}P < 0.01$, compared with Model group. TCA: tricarboxylic acid.

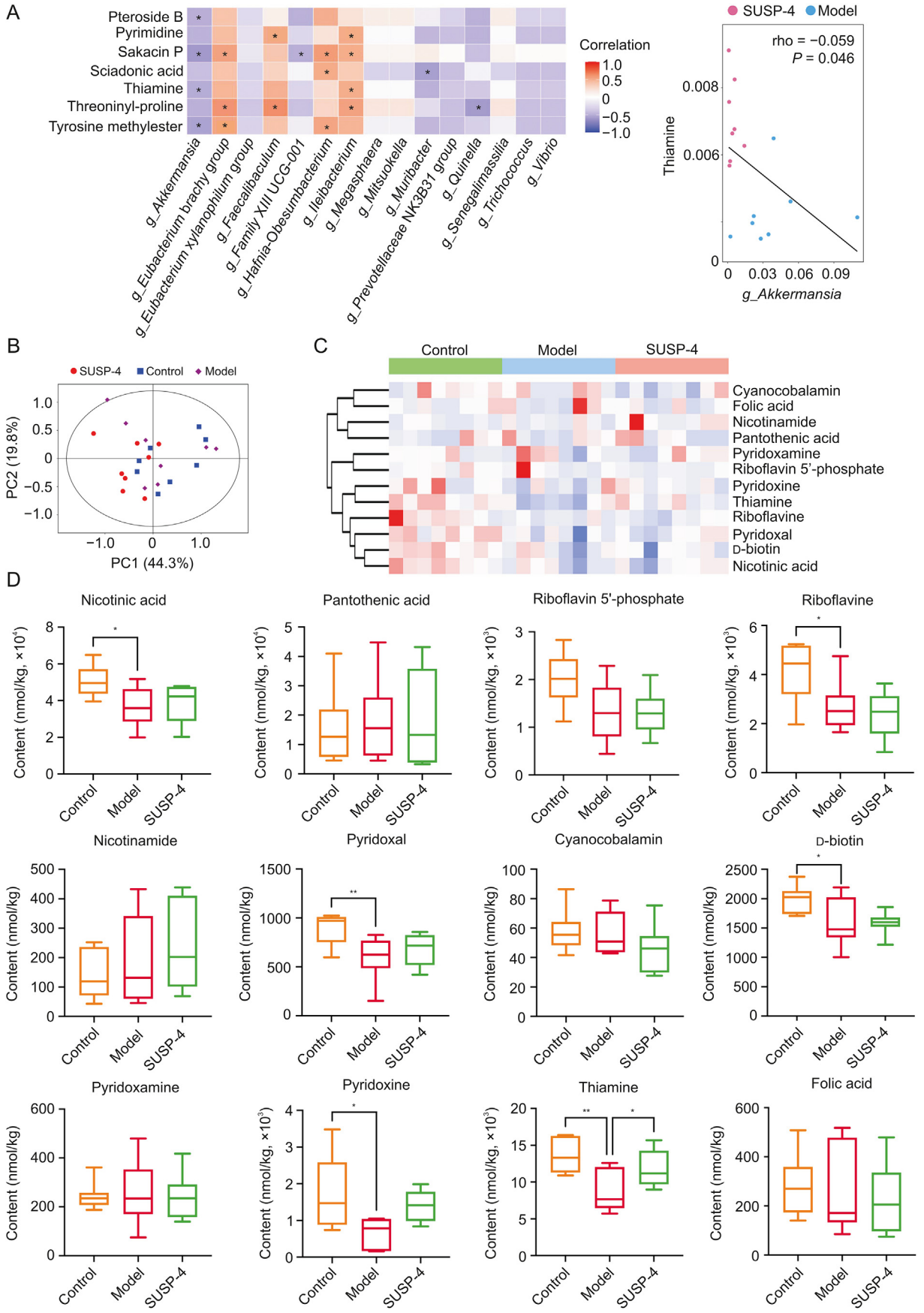

Fig. 9. Conjoint analysis of gut microbiota and metabolites. (A) Conjoint analysis of gut microbiota and metabolites. * Represents a significant correlation. (B) Score scatter plot of principal component analysis (PCA) model for B vitamins-targeted metabolism. (C) Cluster analysis of B vitamins content. (D) Statistics of B vitamins content. Data are presented as the mean ± standard deviation (SD) ($n = 8$). $^{*}P < 0.05$ and $^{**}P < 0.01$, compared with Model group. PC: principal component.

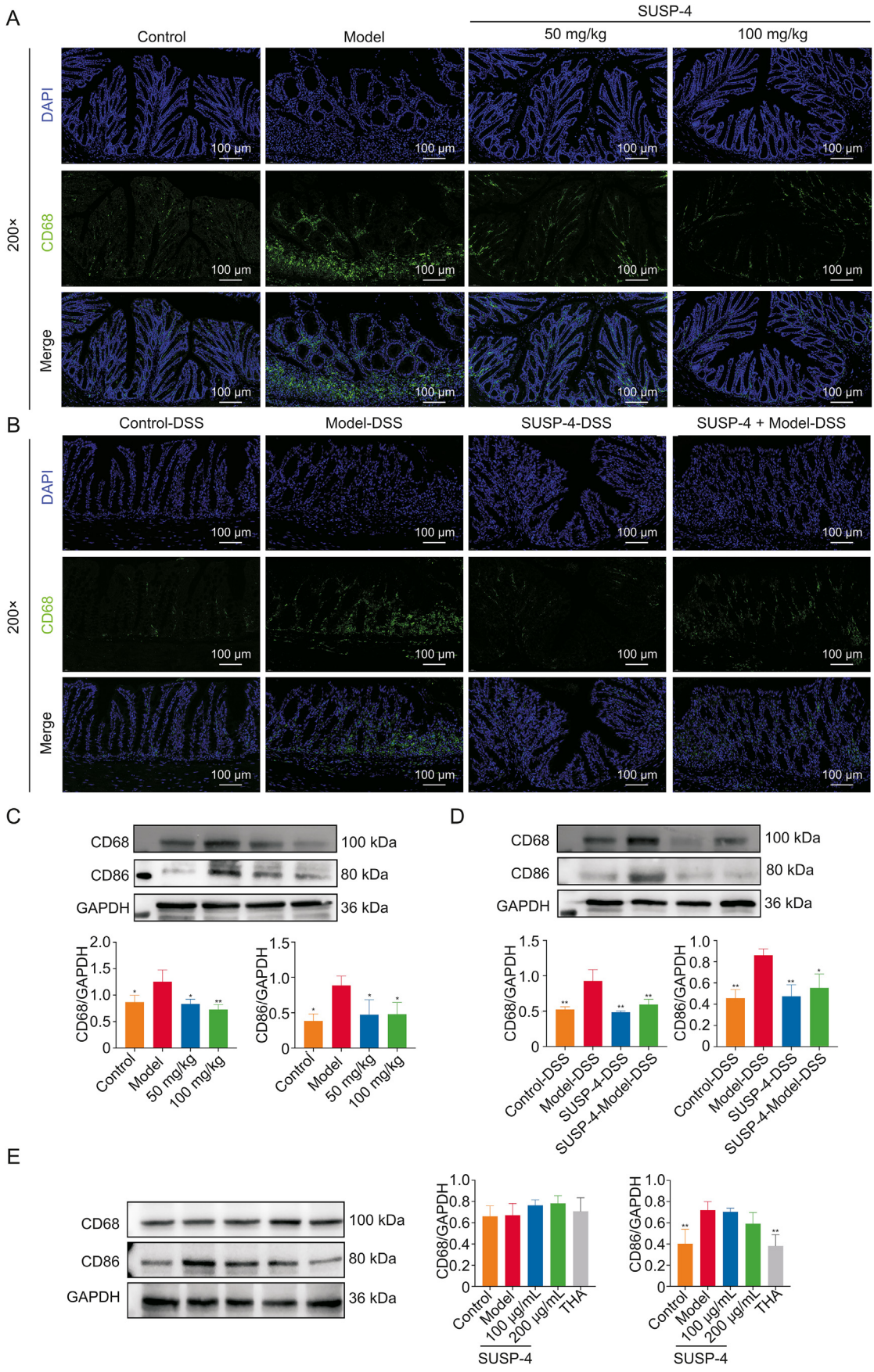
A
SUSP-4
Control
Model
50 mg/kg
100 mg/kg
DAPI
CD68
Merge
200×
100 μm
B
Control-DSS
Model-DSS
SUSP-4-DSS
SUSP-4 + Model-DSS
C
CD68
CD86
GAPDH
100 kDa
80 kDa
36 kDa
CD68/GAPDH
CD86/GAPDH
Control
Model
50 mg/kg
100 mg/kg
D
Control-DSS
Model-DSS
SUSP-4-DSS
SUSP-4-Model-DSS
E
100 μg/mL
200 μg/mL
THA
SUSP-4

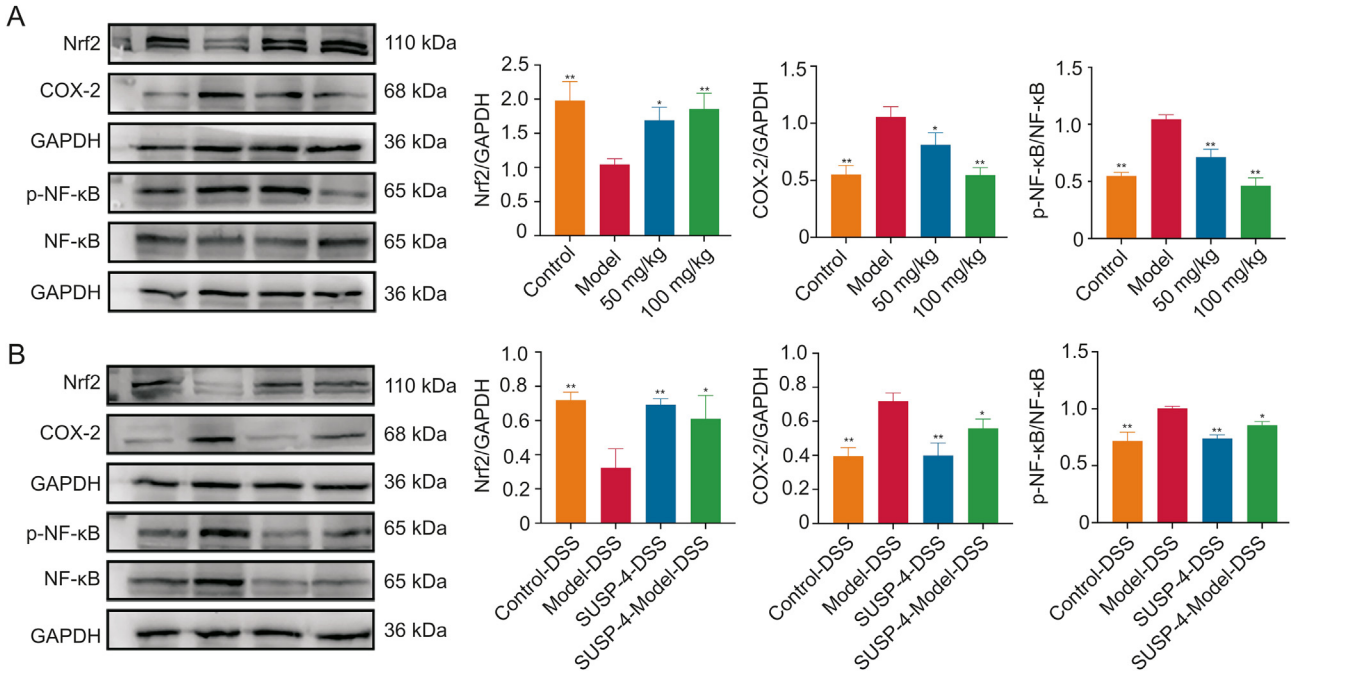

Fig. 11. SUSP-4 regulates the NF-E2-related factor 2 (Nrf2)/cyclooxygenase-2 (COX-2)/phospho-nuclear factor kappa-B (p-NF-κB) pathway. (A) Effects of SUSP-4 on Nrf2, COX-2, and p-NF-κB expression levels. Data are presented as the mean ± standard deviation (SD) ($n = 3$). $^{*}P < 0.05$ and $^{**}P < 0.01$, compared with Model group. (B) Effects of SUSP-4 on Nrf2, COX-2, and p-NF-κB expression levels. Data are presented as the mean ± SD ($n = 3$). $^{*}P < 0.05$ and $^{**}P < 0.01$, compared with Model-DSS group. GAPDH: glyceraldehyde-3-phosphate dehydrogenase; DSS: dextran sulfate sodium.

Muribaculaceae. *Akkermansia*, also known as mucolytic bacteria, has the ability to promote intestinal barrier integrity, modulate immune responses, and suppress inflammation [39]. In many studies, *Akkermansia* abundance was decreased in IBD, but some studies have found that *Akkermansia* overgrowth was followed by degradation of intestinal mucin and direct exposure of intestinal epithelial cells to microorganisms, which may lead to intestinal barrier damage and induce intestinal inflammation [40,41]. Selenium-containing tea polysaccharides [42] and Hericium erinaceus polysaccharides [43] have been shown to ameliorate intestinal inflammation by decreasing the abundance of *Akkermansia*, which was the same as the results of our study. According to the results of the evolutionary branching diagram of linear discriminant analysis effect size (LEfSe), the evolutionary relation of *Akkermansia* at different levels are *Akkermansia*→Akkermansiaceae→Verrucomicrobiales→Verrucomicrobae→Verrucomicrobiota, and SUSP-4 showed a significant downregulation effect, indicating that *Akkermansia* dominated in Verrucomicrobiota. Compared with other genera, SUSP-4 showed the most significant regulation of *Akkermansia*. It was speculated that *Akkermansia* should be one key bacteria in controlling IBD.

The results of FMT showed that the feces given SUSP-4 showed improvement after transplantation to the recipient mice. Compared with Model-DSS mice, the mice in the SUSP-4-DSS and SUSP-4 + Model-DSS groups showed significantly reduced weight fluctuations, improvement in colonic shortening, inhibition of inflammation and oxidative stress, and significant recovery from pathological damage. These data showed that SUSP-4 exerted its effect by improving the intestinal flora.

Metabolism is the main modes of interaction between bacterial and host, and small compounds produced by them play important roles in life activities [44]. In IBD studies, many reports have found that reduced levels of short-chain fatty acids (SCFAs) can promote the development of IBD [45–47]. SCFAs are mainly produced by anaerobic bacteria, and their main effects include improvement of intestinal barrier function, reduction of oxidative stress, and anti-inflammatory and anticancer effects [48,49]. The results of differential metabolite analysis by untargeted metabolomics showed that SUSP-4 significantly downregulated 4,5-dimethyloxazole, *n*-carbamoyl-putrescine, 8,11,14-eicosatrienoic acid, and 4-guan-idinobutanoic acid, and significantly upregulated thiamine, pyrimidine, and 71 other metabolites compared with Model group. The pathway enrichment analysis suggested that the common enriched metabolic pathway in the Control vs. Model and Model vs. SUSP-4 groups was thiamine metabolism. We suggested that SUSP-4 played a role in improving IBD by regulating the thiamine metabolism pathway, and we confirmed that SUSP-4 significantly elevated thiamine levels in the feces of mice based on thiamine-targeted metabolomics analysis.

Based on the results of 16S rRNA sequencing and metabolomics, we performed an association analysis using differential bacteria with differential metabolites and found that *Akkermansia* was markedly negatively correlated with thiamine level, and a correlation consistent with the regulatory role of SUSP-4 for both was found.

It has been shown that thiamine can inhibit macrophage activation to improve the inflammatory response [50]. CD68 and CD86 were markers of macrophages. Among them, CD68 is a universal

Fig. 10. SUSP-4 inhibits macrophage activation. (A, B) Immunofluorescence staining of CD68 in the colon. (C) Effects of SUSP-4 on cluster of differentiation 68 (CD68) and CD86 expression levels in mice. Data are presented as the mean ± standard deviation (SD) ($n = 3$). $^{*}P < 0.05$ and $^{**}P < 0.01$, compared with Model group. (D) Effects of SUSP-4 on CD68 and CD86 expression levels in fecal microbiota transplantation (FMT) test. Data are presented as the mean ± SD ($n = 3$). $^{*}P < 0.05$ and $^{**}P < 0.01$, compared with Model-DSS group. (E) Effects of SUSP-4 and thiamine (THA) on CD68 and CD86 expression levels in RAW264.7. Data are presented as the mean ± SD ($n = 3$). $^{**}P < 0.01$, compared with Model group. DAPI: 4',6-diamidino-2-phenylindole; DSS: dextran sulfate sodium; GAPDH: glyceraldehyde-3-phosphate dehydrogenase.

marker and CD86 is a marker of macrophage M1 type. Activation of macrophages can increase the release of proinflammatory factors [51]. Immunofluorescence and Western blotting results demonstrated that CD68 and CD86 expression levels were markedly increased in Model group, which were significantly downregulated by SUSP-4. We used *in vitro* cell experiments to verify the inhibitory effects of SUSP-4 and thiamine on macrophage activation. The data showed that although SUSP-4 reduced CD86 expression at the concentration of 200 μg/mL, and there was no significant difference compared with Model group. However, thiamine significantly inhibited CD86 expression. Based on these results, we concluded that SUSP-4 had limited direct inhibition effect on macrophage activation, and acted primarily by regulating thiamine levels in the body to suppress macrophage activation. In molecular mechanism experiments, Western blotting experiments showed that SUSP-4 significantly increased Nrf2 level and markedly decreased COX-2 and p-NF-κB levels. The same results were also found in FMT test.

In the fecal samples, we found a significant negative correlation between *Akkermansia* and thiamine based on an association assay. This association was fascinating, and we believed that the increased abundance of *Akkermansia* disrupted the functions of some key proteins on the surface of the gut, thereby exacerbating inflammation and oxidative stress. Simultaneously, the level of thiamine in the body was reduced, which plays a crucial role in intestinal immunity. SUSP-4 had a protective effect by reducing the abundance of *Akkermansia* to promote thiamine metabolism and suppress macrophage activation to inhibit inflammation and oxidative stress. In this study, we found the possible relation between *Akkermansia* and thiamine on regulating IBD, which should be confirmed by further experiments. In addition, the clinical application and deeply mechanisms of SUSP-4 against IBD should also be tested in further.

5. Conclusions

In this work, SUSP-4 was first isolated and identified from *Selaginella uncinata* (Desv.) Spring., and SUSP-4 exerted anti-IBD effects by modulating *Akkermansia* to affect thiamine metabolism and inhibit macrophage activation, which in turn modulated NF-κB/Nrf2/COX-2-mediated inflammation and oxidative stress. All in all, SUSP-4 will play a huge role in the treatment of IBD, whether as a drug or dietary fiber.

CRediT author statement

Haochen Hui: Methodology, Investigation, Writing - Original draft preparation, Visualization; **Zhuoya Wang:** Investigation, Visualization; **Xuerong Zhao:** Investigation, Resources, Supervision; **Lina Xu:** Writing - Reviewing and Editing; **Lianhong Yin:** Formal analysis, Resources, Supervision; **Feifei Wang:** Resources, Funding acquisition, Project administration; **Liping Qu** and **Jinyong Peng:** Supervision, Funding acquisition, Project administration.

Declaration of competing interest

The authors declare that there are no conflicts of interest.

Acknowledgments

The authors gratefully acknowledge the funding from the Spring City Plan of the High-Level Talent Promotion and Training Project of Kunming, China (Grant No.: 2022SCP008) and the Independent Research Fund of Yunnan Characteristic Plant Extraction Laboratory, China (Grant No.: 2022YKZY001).

Appendix A. Supplementary data

Supplementary data to this article can be found online at https://doi.org/10.1016/j.jpha.2023.08.003.

References

[1] G.G. Kaplan, The global burden of IBD: From 2015 to 2025, Nat. Rev. Gastroenterol. Hepatol. 12 (2015) 720–727.
[2] G.P. Ramos, K.A. Papadakis, Mechanisms of disease: Inflammatory bowel diseases, Mayo Clin. Proc. 94 (2019) 155–165.
[3] J. Ni, G.D. Wu, L. Albenberg, et al., Gut microbiota and IBD: Causation or correlation? Nat. Rev. Gastroenterol. Hepatol. 14 (2017) 573–584.
[4] B. Al-Bawardy, R. Shivashankar, D.D. Proctor, Novel and emerging therapies for inflammatory bowel disease, Front. Pharmacol. 12 (2021), 651415.
[5] E.K. Wright, N.S. Ding, O. Niewiadomski, Management of inflammatory bowel disease, Med. J. Aust. 209 (2018) 318–323.
[6] M.R. Kudelka, S.R. Stowell, R.D. Cummings, et al., Intestinal epithelial glycosylation in homeostasis and gut microbiota interactions in IBD, Nat. Rev. Gastroenterol. Hepatol. 17 (2020) 597–617.
[7] J.R. Marchesi, D.H. Adams, F. Fava, et al., The gut microbiota and host health: A new clinical frontier, Gut 65 (2016) 330–339.
[8] J.K. Nicholson, E. Holmes, J. Kinross, et al., Host-gut microbiota metabolic interactions, Science 336 (2012) 1262–1267.
[9] G. Ye, J. Li, J. Zhang, et al., Structural characterization and antitumor activity of a polysaccharide from *Dendrobium wardianum*, Carbohydr. Polym. 269 (2021), 118253.
[10] S. Zhou, G. Huang, G. Chen, Extraction, structural analysis, derivatization and antioxidant activity of polysaccharide from Chinese yam, Food Chem. 361 (2021), 130089.
[11] Y. Liu, Y. Ye, X. Hu, et al., Structural characterization and anti-inflammatory activity of a polysaccharide from the *lignified okra*, Carbohydr. Polym. 265 (2021), 118081.
[12] T. Xia, C.-S. Liu, Y.-N. Hu, et al., Coix seed polysaccharides alleviate type 2 diabetes mellitus via gut microbiota-derived short-chain fatty acids activation of IGF1/PI3K/AKT signaling, Food Res. Int. 150 (2021), 110717.
[13] G. Ma, Q. Xu, H. Du, et al., Characterization of polysaccharide from *Pleurotus eryngii* during simulated gastrointestinal digestion and fermentation, Food Chem. 370 (2022), 131303.
[14] L. Cui, X. Guan, W. Ding, et al., *Scutellaria baicalensis* Georgi polysaccharide ameliorates DSS-induced ulcerative colitis by improving intestinal barrier function and modulating gut microbiota, Int. J. Biol. Macromol. 166 (2021) 1035–1045.
[15] C. Guo, D. Guo, L. Fang, et al., *Ganoderma lucidum* polysaccharide modulates gut microbiota and immune cell function to inhibit inflammation and tumorigenesis in colon, Carbohydr. Polym. 267 (2021), 118231.
[16] C. Guo, Y. Wang, S. Zhang, et al., *Crataegus pinnatifida* polysaccharide alleviates colitis via modulation of gut microbiota and SCFAs metabolism, Int. J. Biol. Macromol. 181 (2021) 357–368.
[17] C. Liu, B. Hu, Y. Cheng, et al., In-depth analysis of the mechanisms of aloe polysaccharides on mitigating subacute colitis in mice via microbiota informatics, Carbohydr. Polym. 265 (2021), 118041.
[18] X.-N. Wu, Y. Yang, H.-H. Zhang, et al., Robustaflavone-4′-dimethyl ether from *Selaginella uncinata* attenuated lipopolysaccharide-induced acute lung injury via inhibiting FLT3-mediated neutrophil activation, Int. Immunopharmacol. 82 (2020), 106338.
[19] J. Xu, L. Yang, R. Wang, et al., The biflavonoids as protein tyrosine phosphatase 1B inhibitors from *Selaginella uncinata* and their antihyperglycemic action, Fitoterapia 137 (2019), 104255.
[20] J. Zheng, Y. Zheng, H. Zhi, et al., Two new steroidal saponins from *Selaginella uncinata* (Desv.) Spring and their protective effect against anoxia, Fitoterapia 88 (2013) 25–30.
[21] H. Hui, M. Gao, X. Zhao, et al., Three water soluble polysaccharides with anti-inflammatory activities from *Selaginella uncinata* (Desv.) Spring, Int. J. Biol. Macromol. 222 (2022) 1983–1995.
[22] Z. Wu, S. Huang, T. Li, et al., Gut microbiota from green tea polyphenol-dosed mice improves intestinal epithelial homeostasis and ameliorates experimental colitis, Microbiome 9 (2021), 184.
[23] E.J. Want, I.D. Wilson, H. Gika, et al., Global metabolic profiling procedures for urine using UPLC-MS, Nat. Protoc. 5 (2010) 1005–1018.
[24] W.B. Dunn, D. Broadhurst, P. Begley, et al., Procedures for large-scale metabolic profiling of serum and plasma using gas chromatography and liquid chromatography coupled to mass spectrometry, Nat. Protoc. 6 (2011) 1060–1083.
[25] T. Kind, G. Wohlgemuth, D.Y. Lee, et al., FiehnLib: Mass spectral and retention index libraries for metabolomics based on quadrupole and time-of-flight gas chromatography/mass spectrometry, Anal. Chem. 81 (2009) 10038–10048.
[26] J. Wang, T. Zhang, X. Shen, et al., Serum metabolomics for early diagnosis of esophageal squamous cell carcinoma by UHPLC-QTOF/MS, Metabolomics 12 (2016), 116.
[27] S. Wang, L. Ni, X. Fu, et al., A sulfated polysaccharide from *Saccharina japonica* suppresses LPS-induced inflammation both in a macrophage cell model via

blocking MAPK/NF-κB signal pathways *in vitro* and a zebrafish model of embryos and larvae *in vivo*, Mar. Drugs 18 (2020), 593.
[28] T. Li, J. Bai, Y. Du, et al., Thiamine pretreatment improves endotoxemia-related liver injury and cholestatic complications by regulating galactose metabolism and inhibiting macrophage activation, Int. Immunopharmacol. 108 (2022), 108892.
[29] S.F. Barbieri, S. da Costa Amaral, E. Mazepa, et al., Isolation, NMR characterization and bioactivity of a (4-*O*-methyl-α-D-glucurono)-β-D-xylan from *Campomanesia xanthocarpa* Berg fruits, Int. J. Biol. Macromol. 207 (2022) 893–904.
[30] T. Komatsu, J. Kikuchi, Comprehensive signal assignment of ^{13}C-labeled lignocellulose using multidimensional solution NMR and ^{13}C chemical shift comparison with solid-state NMR, Anal. Chem. 85 (2013) 8857–8865.
[31] Z. Sheng, L. Wen, B. Yang, Structure identification of a polysaccharide in mushroom Lingzhi spore and its immunomodulatory activity, Carbohydr. Polym. 278 (2022), 118939.
[32] K. Zhao, B. Li, D. He, et al., Chemical characteristic and bioactivity of hemicellulose-based polysaccharides isolated from *Salvia miltiorrhiza*, Int. J. Biol. Macromol. 165 (2020) 2475–2483.
[33] A.A. de Sousa, N.M Benevides, A. de Freitas Pires, et al., A report of a galactan from marine alga *Gelidium crinale* with *in vivo* anti-inflammatory and anti-nociceptive effects, Fundam. Clin. Pharmacol. 27 (2013) 173–180.
[34] M. Zou, X. Hu, Y. Wang, et al., Structural characterization and anti-inflammatory activity of a pectin polysaccharide HBHP-3 from *Houttuynia cordata*, Int. J. Biol. Macromol. 210 (2022) 161–171.
[35] M. Argollo, D. Gilardi, C. Peyrin-Biroulet, et al., Comorbidities in inflammatory bowel disease: A call for action, Lancet Gastroenterol. Hepatol. 4 (2019) 643–654.
[36] B. Chami, N.J.J. Martin, J.M. Dennis, et al., Myeloperoxidase in the inflamed colon: A novel target for treating inflammatory bowel disease, Arch. Biochem. Biophys. 645 (2018) 61–71.
[37] A. Dos Santos Ramos, G.C.S. Viana, M. de Macedo Brigido, et al., Neutrophil extracellular traps in inflammatory bowel diseases: Implications in pathogenesis and therapeutic targets, Pharmacol. Res. 171 (2021), 105779.
[38] K. Matsuoka, T. Kanai, The gut microbiota and inflammatory bowel disease, Semin. Immunopathol. 37 (2015) 47–55.
[39] P.D. Cani, C. Depommier, M. Derrien, et al., *Akkermansia muciniphila*: Paradigm for next-generation beneficial microorganisms, Nat. Rev. Gastroenterol. Hepatol. 19 (2022) 625–637.
[40] C. Belzer, L.W. Chia, S. Aalvink, et al., Microbial metabolic networks at the mucus layer lead to diet-independent butyrate and vitamin B_{12} production by intestinal symbionts, mBio 8 (2017), e00770-17.
[41] R. Caesar, V. Tremaroli, P. Kovatcheva-Datchary, et al., Crosstalk between gut microbiota and dietary lipids aggravates WAT inflammation through TLR signaling, Cell Metab. 22 (2015) 658–668.
[42] Y. Zhao, H. Chen, W. Li, et al., Selenium-containing tea polysaccharides ameliorate DSS-induced ulcerative colitis via enhancing the intestinal barrier and regulating the gut microbiota, Int. J. Biol. Macromol. 209 (2022) 356–366.
[43] Y. Ren, Y. Geng, Y. Du, et al., Polysaccharide of *Hericium erinaceus* attenuates colitis in C57BL/6 mice via regulation of oxidative stress, inflammation-related signaling pathways and modulating the composition of the gut microbiota, J. Nutr. Biochem. 57 (2018) 67–76.
[44] M.M. Rinschen, J. Ivanisevic, M. Giera, et al., Identification of bioactive metabolites using activity metabolomics, Nat. Rev. Mol. Cell Biol. 20 (2019) 353–367.
[45] L. Su, C. Mao, X. Wang, et al., The anti-colitis effect of *Schisandra chinensis* polysaccharide is associated with the regulation of the composition and metabolism of gut microbiota, Front. Cell. Infect. Microbiol. 10 (2020), 519479.
[46] Y. Sun, L. Fan, W. Mian, et al., Modified apple polysaccharide influences MUC-1 expression to prevent ICR mice from colitis-associated carcinogenesis, Int. J. Biol. Macromol. 120 (2018) 1387–1395.
[47] Y. Wang, N. Zhang, J. Kan, et al., Structural characterization of water-soluble polysaccharide from *Arctium lappa* and its effects on colitis mice, Carbohydr. Polym. 213 (2019) 89–99.
[48] B. Dalile, L. Van Oudenhove, B. Vervliet, et al., The role of short-chain fatty acids in microbiota-gut-brain communication, Nat. Rev. Gastroenterol. Hepatol. 16 (2019) 461–478.
[49] D. Parada Venegas, M.K. De la Fuente, G. Landskron, et al., Short chain fatty acids (SCFAs)-mediated gut epithelial and immune regulation and its relevance for inflammatory bowel diseases, Front. Immunol. 10 (2019), 277.
[50] K.L. Ford, D.J. Jorgenson, E.J.L. Landry, et al., Vitamin and mineral supplement use in medically complex, community-living, older adults, Appl. Physiol. Nutr. Metab. 44 (2019) 450–453.
[51] L. Chávez-Galán, M.L. Olleros, D. Vesin, et al., Much more than M1 and M2 macrophages, there are also $CD169^+$ and TCR^+ macrophages, Front. Immunol. 6 (2015), 263.